Submitted to Journal Low
Temperture Physics

LBL-6243
Preprint
UC-37 and UC-38

DC SQUID: NOISE AND OPTIMIZATION

Claudia D. Tesche and John Clarke

May 1977

Prepared for the U. S. Energy Research and
Development Administration under Contract 7405-ENG-48

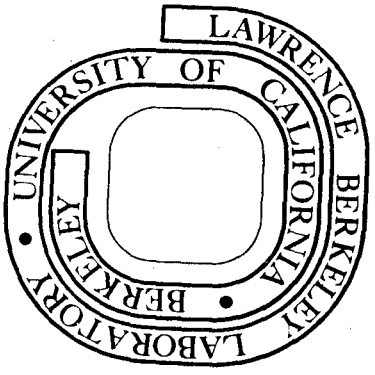

DISCLAIMER

To be submitted to J. Low Temp. Phys.

LBL-6243

DC SQUID: NOISE AND OPTIMIZATION*

Claudia D. Tesche and John Clarke

Department of Physics, University of California
and Materials and Molecular Research Division
Lawrence Berkeley Laboratory, Berkeley, California 94720

---

*Work supported by the U.S.E.R.D.A.

ABSTRACT

A computer model is described for the dc SQUID in which the two Josephson junctions are non-hysteretic resistively shunted tunnel junctions. In the absence of noise, current-voltage (I-V) characteristics are obtained as functions of the applied flux, Φ_a, SQUID inductance, L, junction critical current, I_o, and shunt resistance, R. The effects of asymmetry in L, I_o, and R are discussed. I-V characteristics, flux-voltage transfer functions, and low frequency spectral densities of the voltage noise are obtained at experimentally interesting values of the parameters in the presence of Johnson noise in the resistive shunts. The transfer functions and voltage spectral densities are used to calculate the flux and energy resolution of the SQUID operated as an open-loop, small signal amplifier. The resolution of the SQUID with ac flux modulation is discussed. The flux resolution calculated for the SQUID of Clarke, Goubau, and Ketchen is $1.6 \times 10^{-5}\ \Phi_o\ \mathrm{Hz}^{-\frac{1}{2}}$, approximately one-half the experimental value. Optimization of the SQUID resolution is discussed: It is shown that the optimum operating condition is $\beta = 2LI_o/\Phi_o \approx 1$. Finally, some speculations are made on the ultimate performance of the tunnel junction dc SQUID. When the dominant noise source is Johnson noise in the resistive shunts, the energy resolution per Hz is $4k_BT(\pi LC)^{\frac{1}{2}}$, where C is the junction capacitance, and the constraint $R = (\Phi_o/2\pi CI_o)^{\frac{1}{2}}$ has been imposed. This result implies that the energy resolution is proportional to (junction area)$^{\frac{1}{2}}$. In the limit $eI_oR \gg k_BT$, the dominant noise source is shot noise in the junctions; for $\beta = 1$, the energy resolution per Hz is then approximately h/2.

1. INTRODUCTION

The dc SQUID[1] (Superconducting QUantum Interference Device) is a sensitive detector of changes in magnetic flux. The resolution of the Josephson tunnel junction device of Clarke, Goubau, and Ketchen [2] is limited by Johnson noise in the resistive shunts used to eliminate hysteresis in the current-voltage characteristics. Approximate expressions[2,3] for the flux resolution as a function of device parameters can be obtained in the limits $\beta = 2LI_o/\Phi_o \gg 1$ or $\beta \ll 1$, where L is the SQUID inductance, and I_o is the critical current of each junction. However, most SQUIDs are operated with $2LI_o/\Phi_o \sim 1$, for which value no detailed calculations of the flux resolution are available. Thus, a proper optimization of the SQUID performance has not been possible.

Previous calculations of the behavior of the dc SQUID have been concerned mostly with the noise-free properties in the zero voltage state. For example, the dependence of the critical current on applied external flux has been investigated by Jaklevic, Lambe, Silver, and Mercereau,[1] Zimmerman and Silver,[4] Schulz-DuBois,[5] and by De Waele and De Bruyn Ouboter[6,7] for the symmetric SQUID, by Fulton,[8] Clarke and Paterson,[9] and Tsang and Van Duzer[10] for asymmetric SQUID, and by Fulton, Dunkleburger and Dynes,[11] and Tsang and Van Duzer[12] for the SQUID with non-sinusoidal current-phase relationships. A qualitative discussion of the noise-free current-voltage characteristic for the SQUID in the small inductance limit has been given by De Waele and De Bruyn Ouboter,[6] and by Tinkham.[3] However, no quantitative calculation of the flux dependence of the current-voltage characteristics has previously been made.

After briefly reviewing the relationship between critical current and applied flux, we calculate numerically noise-free current-voltage characteristics for the symmetric and asymmetric SQUID as a function of the device parameters. Next, we extend the calculation to include explicitly the voltage noise sources associated with the shunt resistances. Noise-rounded current-voltage characteristics are obtained for the single shunted junction and compared with those computed by Auracher[13] using a similar technique, and by Ambegaokar and Halperin[14] and by Fulton[15] using different methods. The agreement is excellent. In addition, computed voltage power spectral densities for the single junction agree well with those computed by Vystavkin et al.[16] by another method. We then compute noise-rounded current-voltage characteristics and voltage spectral densities for experimentally interesting values of the SQUID parameters and determine the flux and energy resolution. The values computed for $\beta >> 1$ and $\beta << 1$ are in excellent agreement with those obtained from approximate expressions. The measured energy resolution of the dc SQUID of Clarke et al.[2] ($\beta \sim 2.5$), approximately 4×10^{-30} JHz^{-1}, is within a factor of two of the calculated value.

Finally, we discuss the optimization of the SQUID. For the case in which the SQUID is operated in a flux-locked loop with an ac flux modulation, we find an optimal value of $\beta \approx 1$. As an example of optimization, we consider possible improvements in the tunnel junction dc SQUID of Clarke et al.[2] If the inductance were lowered by a factor of 3 to 0.3 nH, and the junction capacitance were lowered by a factor of 200 by decreasing the junction area, the energy resolution would be increased by a factor of about 15. We speculate that the ultimate energy resolution of the SQUID

may be limited by the shot noise in the junctions to a value given by the uncertainty principle, and that is four orders of magnitude higher than that presently achieved experimentally.

A brief preliminary report of this work has appeared elsewhere.[17]

2. EQUATIONS FOR THE DC SQUID

Our model for the dc SQUID[1] consists of two resistively shunted Josephson junctions[18] mounted on a superconducting ring (see Fig. 1). We derive a set of equations describing the time-dependent behavior of the SQUID, including the effects of the Johnson noise associated with the shunts. For the general case of an asymmetric SQUID, the critical currents of the two junctions are $(1 - \alpha)I_o$ and $(1 + \alpha)I_o$ $(|\alpha| \leq 1)$. The shunt resistances are $R/(1 - \rho)$ and $R/(1 + \rho)$ $(|\rho| < 1)$. The self inductances of the two arms are L_1 and L_2, the mutual inductance between the arms is M, and the ring inductance is L. The constant bias current is I, and the time-dependent currents in each arm are $I_1(t)$ and $I_2(t)$. Thus

$$I = I_1 + I_2 \ . \tag{2.1}$$

We define the circulating current J(t) to be

$$J = (I_2 - I_1)/2 \ . \tag{2.2}$$

We assume that the flux threading each junction is always much less than a flux quantum, Φ_o, and that the currents flowing through the junctions obey the Josephson current-phase relation. The currents $I_1(t)$ and $I_2(t)$ are related to the voltages $V_1(t)$ and $V_2(t)$ and phase differences $\delta_1(t)$ and $\delta_2(t)$ across the junctions by

$$I_1 = (1 - \alpha)I_o \sin\delta_1 + (1 - \rho)(V_1 - V_{N1})/R \ , \tag{2.3}$$

and

$$I_2 = (1 + \alpha)I_o \sin\delta_2 + (1 + \rho)(V_2 - V_{N2})/R \ . \tag{2.4}$$

Here, V_{N1} and V_{N2} are the time-dependent Johnson noise voltages in series with the shunt resistors. The phase differences develop in time according

to the voltage-frequency relations

$$d\delta_1/dt = (2e/\hbar)V_1 \ , \tag{2.5}$$

and

$$d\delta_2/dt = (2e/\hbar)V_2 \ . \tag{2.6}$$

The total voltage V developed across the SQUID is

$$V = V_1 + L_1 dI_1/dt + M dI_2/dt \ , \tag{2.7}$$

and

$$V = V_2 + L_2 dI_2/dt + M dI_1/dt \ . \tag{2.8}$$

The phase differences δ_1 and δ_2 are related by[4]

$$\delta_1 - \delta_2 = 2\pi\Phi_T/\Phi_o \ , \tag{2.9}$$

where Φ_T is the total flux threading the superconducting ring. The total flux is the sum of the individual fluxes Φ_1 and Φ_2 produced by the currents I_1 and I_2 and the externally applied quasistatic flux, Φ_a. We can restrict Φ_a to the range $0 \leq \Phi_a \leq \Phi_o$ without loss of generality since all SQUID responses are periodic in Φ_a with period Φ_o. The fluxes Φ_1 and Φ_2 are proportional to the currents I_1 and I_2. Defining $\mathcal{L}_1 = -\Phi_1/I_1$ and $\mathcal{L}_2 = +\Phi_2/I_2$ we can easily show that $\mathcal{L}_1 + \mathcal{L}_2 = L$; we take $\mathcal{L}_1 = (1 - \eta)L/2$ and $\mathcal{L}_2 = (1 + \eta)L/2$ $(|\eta| \leq 1)$. The total flux thus becomes

$$\Phi_T = \Phi_a + LJ + \eta LI/2 \ , \tag{2.10}$$

where we have used Eqs. (2.1) and (2.2). The geometric quantities L, L_1, L_2, $\mathcal{L}_1$, $\mathcal{L}_2$, and M are related in the following way. Suppose that in some time-dependent mode $dI_1/dt \neq 0$ and $dI_2/dt = 0$. The inductive voltage drop around the entire loop (neglecting any contributions from the junctions or shunts) is $V = L_1 dI_1/dT - M dI_1/dT$. The rate of change of flux in the ring yields $V = \mathcal{L}_1 dI_1/dt$ (again ignoring any flux contributions from the junctions or shunts). Hence $\mathcal{L}_1 = L_1 - M$, and, similarly, $\mathcal{L}_2 = L_2 - M$. Using these

expressions for M and the fact that $dJ/dt = - dI_1/dt = dI_2/dt$ (since I is constant), we can reduce Eqs. (2.7) and (2.8) to

$$V = V_1 - (1 - \eta) \frac{L}{2} \frac{dJ}{dt} , \tag{2.11}$$

and

$$V = V_2 + (1 + \eta) \frac{L}{2} \frac{dJ}{dt} . \tag{2.12}$$

These equations include the effect of the mutual inductance even though M does not appear explicitly.

The final set of equations for J and V in terms of the bias current I, the applied flux Φ_a, the noise voltages V_{N1} and V_{N2}, and the SQUID parameters I_o, R, L, α, ρ, and η are obtained from Eqs. (2.1)-(2.12) by eliminating I_1, I_2, V_1, and V_2. For convenience, we use the following dimensionless units: voltage in units of I_oR, current in units of I_o, flux in units of Φ_o, and time θ in units of $\Phi_o/2\pi I_oR$. The dimensionless quantitites are expressed in lower case letters. We define $\beta = 2LI_o/\Phi_o$. Hence from Eqs. (2.9) and (2.10):

$$j = (\delta_1 - \delta_2 - 2\pi\phi_a)/\pi\beta - \eta i/2 ; \tag{2.13}$$

from Eqs. (2.5)-(2.12):

$$v = \frac{(1 + \eta)}{2} \frac{d\delta_1}{d\theta} + \frac{(1 - \eta)}{2} \frac{d\delta_2}{d\theta} ; \tag{2.14}$$

and from Eqs. (2.1) to (2.6):

$$\frac{d\delta_1}{d\theta} = \frac{i/2 - j - (1 - \alpha) \sin\delta_1}{1 - \rho} + v_{N1} , \tag{2.15}$$

and

$$\frac{d\delta_2}{d\theta} = \frac{i/2 + j - (1 + \alpha) \sin\delta_2}{1 + \rho} + v_{N2} . \tag{2.16}$$

Equations (2.13)-(2.16) can also be used to describe the behavior of the SQUID shown in Fig. 1(b). This configuration is used in the SLUG,[19] and the thin film gradiometer.[20] In this case, the applied flux is coupled to the SQUID by means of a signal current, I_s. In Appendix A, we show that ϕ_a and j must be replaced by $-(1-\xi)\beta i_s/4$ and $(j_T + i_s/2)$ respectively, where j_T is the total circulating current, and ξ describes the asymmetry in the upper and lower arms of the SQUID. With these substitutions, all of the enusing results can be applied to SQUIDs in this configuration. In particular, the critical current and voltage across the SQUID are periodic in the signal current with period $(1 - \xi)LI_s/2$.

3. SQUID CHARACTERISTICS IN THE ABSENCE OF NOISE

In this section we discuss the behavior of the SQUID in the absence of noise. We thus set $v_{N1} = v_{N2} = 0$ in Eqs. (2.15) and (2.16).

3.1 Case I: $v = 0$

Consider first the case in which the bias current i is sufficiently low that no voltage is produced across the SQUID. The largest such current, i_c, is a function of α, β, η, and ϕ_a. Although curves of $i_c(\phi_a)$ have appeared previously in the literature,[5-12] for future reference, we include here plots of i_c vs. ϕ_a for various values of α, β, and η. For $v = 0$, we can set the time derivatives in Eqs. (2.13)-(2.16) equal to zero to obtain

$$i = (1 - \alpha)\sin\delta_1 + (1 + \alpha)\sin\delta_2 , \tag{3.1}$$

$$2j = -(1 - \alpha)\sin\delta_1 + (1 + \alpha)\sin\delta_2 , \tag{3.2}$$

and

$$\delta_2 = \delta_1 - 2\pi\phi_a - \pi\beta j - \pi\beta\eta i/2 . \tag{3.3}$$

Eqs. (3.1) to (3.3) are independent of the shunt imbalance, ρ, as we expect for $v = 0$. We computed the variation of i_c with ϕ_a by numerically solving these equations* (see Appendix B).

Curves of i_c vs. ϕ_a for variable α and η with $\beta = 1.0$ appear in Figs. 2(a) and 2(b) respectively. Equations (3.1)-(3.3) imply that i_c attains the maximum value, 2.0, for some ϕ_a whatever the values of α, η, and β. With $\delta_1 = \delta_2 = \pi/2$, we have $j = \alpha$ and $\phi_a = -\beta(\alpha + \eta)/2$ at that point. The values of i_c at other values of ϕ_a depend on η and α in the following manner. With $\eta = 0$, the modulation depth, $\Delta i_c = i_{c\,max} - i_{c\,min}$, falls to

*An elegant alternative method of solution has been given by Tsang and Van Duzer.[10]

zero as α is increased from 0 to 1. In addition, the value of ϕ_a at which $i_{c\,min}$ occurs shifts away from 0.5 as the SQUID asymmetry increases. In the limit $|\alpha| = 1$, $i_c = 2$ for all ϕ_a. It should be noted that in the large β limit, Δi_c is much less sensitive to the value of α: Zimmerman and Silver[4] demonstrated experimentally that Δi_c becomes significantly reduced only when the critical current of one of the junctions fall below $\Delta i_c(\alpha = 0)$.

The modulation Δi_c is independent of the value of η, as can be seen from Fig. 2(b). For $\alpha = 0$, the value of ϕ_a at $i_{c\,min}$ is shifted from $\phi_a = 0.5$ for $\eta = 0$ to $\phi_a = 0.5 - \beta\eta i_{c\,min}/4$ for $\eta \neq 0$. In fact, the entire i_c vs. ϕ_a curve for arbitrary η can be readily generated from the corresponding $\eta = 0$ curve. A particular value of i_c at ϕ_a^o for $\eta = 0$ will occur at $\phi_a^\eta = \phi_a^o - \beta\eta i_c/4$ for $\eta \neq 0$. Since the amount by which ϕ_a^η is shifted increases with i_c, the $\eta \neq 0$ curves appear skewed (see Appendix C for a proof).

Curves of i_c vs. ϕ_a for various values of β with $\alpha = \eta = 0$ are plotted in Fig. 3. Similar curves have been published elsewhere.[21]

Let $\Delta I_c = 2I_o - I_c(\Phi_o/2)$ be the modulation depth in dimensioned units. We display the dependence of ΔI_c on the parameters L and I_o in Fig. 4. For variable L and fixed I_o, the modulation depth is expressed in dimensionless units as $(\Delta I_c/2I_o)$, and plotted vs. $\beta = L(2I_o/\Phi_o)$ in Fig. 4(a). As L is reduced below a value corresponding to $\beta \approx 0.1$, ΔI_c approaches the limit $2I_o$ independent of L. Hence decreasing the SQUID inductance below $0.1\ \Phi_o/2I_o$ has little effect on ΔI_c.

The dependence of ΔI_c on I_o for fixed SQUID inductance L is plotted in Fig. 4(b). Here, the modulation depth is plotted as the dimensionless parameter $\Delta I_c/(\Phi_o/L)$ vs. $\beta = I_o(2L/\Phi_o)$. For $\beta \gtrsim 40$, $\Delta I_c \approx \Phi_o/L$. Thus the modulation depth approaches a limit independent of I_o for sufficiently

large values of I_o. The experimental points shown were obtained by Clarke and Paterson using a SQUID with SNS junctions.[22] The agreement is excellent.

3.2 Case II: $v > 0$

When the SQUID is biased at a constant current $i > i_c$, the circulating current j and voltage v oscillate in time. We integrate Eqs. (2.13) to (2.16) stepwise in time to determine the dependence of $v(\theta)$ and $j(\theta)$ on α, β, η, ρ, and ϕ_a. The initial conditions are chosen to minimize the transient response of the SQUID. The results shown for $v(\theta)$ and $j(\theta)$ are taken after several oscillations, and thus reflect the steady state behavior corresponding to the state of least energy of the SQUID. Fig. 5 shows $v(\theta)$ and $j(\theta)$ vs. time for several values of the SQUID parameters. The period of oscillation for $v(\theta)$ is $\tau = 2\pi/\bar{v}$ in all cases, where $\bar{v}$ is the time-averaged voltage. For the special case of a completely symmetric SQUID ($\alpha = \eta = \rho = 0$) at $\phi_a = 0$, $j(\theta) \equiv 0$. For the symmetric SQUID at $\phi_a = 0.5$, $j(\theta)$ oscillates symmetrically about zero with period $\tau/2$. For all other cases, the current $j(\theta)$ also oscillates with the period τ of the voltage oscillations. For bias currents very near i_c, $v(\theta)$ and $j(\theta)$ exhibit sharp spikes, indicating the presence of many higher harmonics of the fundamental frequency. As i is increased, $v(\theta)$ and $j(\theta)$ become progressively more sinusoidal. This behavior is very similar to that observed in single junctions.[23]

The curves of voltage vs. time can be averaged over a complete cycle to yield i-$\bar{v}$ characteristics as functions of the various SQUID parameters. In Fig. 6(a) we plot i-$\bar{v}$ characteristics for the symmetric SQUID with $\beta = 1.0$ for several values of ϕ_a. The effect of changing β on the i-$\bar{v}$ characteristics for $\phi_a = 0.5$ is seen in Fig. 6(b). As i increases, the characteristics approach the equivalent single junction curve (represented

in Fig. 6(a) as $\phi_a = 0$, and in Fig. 6(b) as $\beta \sim \infty$). Hence the SQUID voltage becomes essentially independent of the applied flux, ϕ_a, for large values of i ($i \gtrsim 4.0$). At lower values of i, the presence of instantaneous circulating currents through the junctions for $\phi_a \neq 0$ produces an increase in $\bar{v}$ over the single junction value.

The dependence of the average $\bar{v}$ and average circulating current $\bar{j}$ on ϕ_a for the symmetric SQUID for various values of β at $i = 2.1$ is shown in Fig. 7. We see that $\bar{j} = 0$ for $\phi_a = 0$ and 0.5 only.

The dependence of the i-$\bar{v}$ characteristics and the curves of $\bar{j}$ vs. ϕ_a and $\bar{v}$ vs. ϕ_a on the degree of SQUID asymmetry is shown in Fig. 8 for $\beta = 1$. Notice that the discontinuity in slope in the i_c vs. ϕ_a curves is not present in the $\bar{v}$ vs. ϕ_a curves. Consider first the family of curves [Figs. 8(a)-(c)] for $\eta \neq 0$. The curves of $\bar{j}$ and $\bar{v}$ vs. ϕ_a with $\eta \neq 0$ are found by shifting the curves for $\eta = 0$ by flux $- \eta\beta i/4$ (see Appendix C). Since the shift is proportional to i, the i-$\bar{v}$ characteristics for $\eta \neq 0$ cannot be generated by a simple shift of the $\eta = 0$ characteristics.

The i-$\bar{v}$ characteristics for $\phi_a = 0.5$, and curves of $\bar{j}$ and $\bar{v}$ vs. ϕ_a for $i = 2.1$ are plotted in Fig. 8(d)-(f) for several values of α, the critical current imbalance. As $|\alpha| \to 1$, the i-$\bar{v}$ characteristic becomes independent of ϕ_a, and approaches the single junction characteristic. This behavior can also be seen in $\bar{v}$ vs. ϕ_a [Fig. 8(f)]. In addition, as $|\alpha| \to 1$, $\bar{j}$ increases for all values of ϕ_a.

The curves in Fig. 8(g)-(i) for various values of ρ show the effects of an imbalance in the shunt resistances. For $\phi_a = 0.5$, the i-$\bar{v}$ characteristics are relatively independent of ρ. This insensitivity to ρ is reflected in the $\bar{v}$ vs. ϕ_a curves. However, the curves of $\bar{j}$ vs. ϕ_a are relatively sensitive to the value of ρ; in the limit of large i, $\bar{j}$ approaches $i\rho/2$.

3.3 Discussion

We conclude that the behavior of the dc SQUID is relatively insensitive to quite large asymmetries in the inductance of the two arms, in the critical currents, or in shunt resistances of the two junctions, provided that neither critical current falls below $\Delta i_c(\alpha = 0)$. Consequently, it appears that near-optimum performance can be achieved with a wide range of values of η, α, and ρ. In the remainder of the paper, we will be concerned only with the symmetric case $\eta = \alpha = \rho = 1$.

4. SQUID CHARACTERISTICS IN THE PRESENCE OF NOISE

In this section we discuss the behavior of the SQUID in the presence of Johnson noise generated in the resistive shunts. We first discuss our numerical techniques. As a check on these techniques, we show that our results for the noise-rounded $i-\bar{v}$ characteristics and voltage noise spectral densities for a single shunted junction are in good agreement with work previously published.[15,16] We then compute the $i-\bar{v}$ characteristics, voltage noise spectral density, and flux resolution of the SQUID as functions of the relevant parameters.

4.1 Numerical Techniques

We assume that the Johnson noise voltages across the external shunt resistances dominate any other source of noise in the SQUID, for example, shot noise in the junctions[24,25], or thermal fluctuations in the critical current[26]. The voltage noise sources v_{N1} and v_{N2} in Eqs. (2.13)-(2.16) are then uncorrelated, each having a white voltage spectral density, $S_V^N = 4k_BTR$, or, in dimensionless units, $S_v^N = 4\Gamma$, where[16] $\Gamma = 2\pi k_BT/I_o\phi_o$. We approximate the random voltages $v_N(\theta)$ by trains of voltage pulses each of duration $\Delta\theta$ and random amplitude v_k. We have used two different techniques to generate the v_k. In Method I we generate a pseudo-random set of Gaussian distributed v_k. We then integrate Eqs. (2.13)-(2.16) using a simple integration routine. The resultant $v(\theta)$ is used to calculate noise-rounded $i-\bar{v}$ characteristics. Unfortunately, as we shall discuss, the calculation of spectral densities from these $v(\theta)$ requires large amounts of computer time. In Method II we use an approximation for the

v_k that reduces significantly the computation time for the spectral densities.

Method I. We use a pseudo-random number generator to generate a Gaussian-distributed set v_k of zero mean with $\langle v_k^2 \rangle = 2\Gamma/\Delta\theta$. The computed power spectrum of the voltage pulses averaged over many sets v_k is white and tends to a constant, 4Γ, as required. Two independent trains of voltage pulses are used to approximate v_{N1} and v_{N2} in Eqs. (2.13)-(2.16). We integrate the phases $\delta_1(\theta)$ and $\delta_2(\theta)$ using an iterative scheme $\delta(\theta + \Delta\theta) = \delta(\theta) + \Delta\theta\ d\delta/d\theta$. The value of $\Delta\theta$ is chosen so that $\Delta\theta\ d\delta/d\theta \ll 2\pi$. The noise-rounded i-$\bar{v}$ characteristics labeled Method I in Figs. 11(a) and 12(a) and the transfer functions in Fig. 13 were generated by time-averaging $v(\theta)$ computed in this way. We estimate that the results are accurate to ± 5%.

Spectral densities, S_v, can be calculated directly from the $v(\theta)$ generated by Method I. N values of $v(\theta)$ at equal time steps $\Delta\theta$ can be used to calculate S_v at frequency intervals $\delta f = 1/N\Delta\theta$. For the case of a single shunt resistance ($i_c = 0$), the values of $v(\theta)$ are just the v_k, and the spectral density (averaged over many sets of v_k) tends to 4Γ as required. We shall be interested in computing spectral densities for the single junction and the SQUID from values of $v(\theta)$ sampled at time intervals corresponding to $n\Delta\theta$ (n is an integer). In those cases, the averaged spectral density for a single shunt resistance is white with a magnitude $n4\Gamma$. The additional factor n is a result of the normalization of the v_k. For v_k defined over time steps $\Delta\theta$, $\langle v_k^2 \rangle = 2\Gamma/\Delta\theta$, while for v_k defined over $n\Delta\theta$, $\langle v_k^2 \rangle = 2\Gamma/n\Delta\theta$. Hence generating v_k over time steps $\Delta\theta$ and sampling the resultant $v(\theta)$ over time steps $n\Delta\theta$ increases the spectral

density by a factor n. It is important to notice that this simple relationship will not hold in general for the case of the single shunted junction or SQUID, since in the limit $\Gamma \to 0$ those spectral densities must be independent of n. Hence to obtain results for S_v that are consistent in both the noise-dominated and noise-free limits, we must take n = 1.

The restriction n = 1 limits our ability to calculate spectral densities efficiently from $v(\theta)$ when $v(\theta)$ is generated by Method I. To see this, we briefly discuss the general behavior of the spectral density for $i \neq 0$, $\Gamma \neq 0$. The spectral density contains noise-broadened peaks at the fundamental Josephson frequency $f_J = \bar{v}/2\pi$ and its harmonics. We are interested in computing the low frequency spectral density, S_v^o, at frequencies well below f_J, where the spectral density is white. As the bias current, i, is lowered towards i_c the harmonics become more important, and, as $\Gamma(T)$ is increased from zero, the broadening increases. Thus, for $i \sim i_c$, and for experimentally interesting values of Γ, S_v must be computed for frequencies well above and well below f_J. However, the lowest frequency is $\delta f = 1/N\Delta\theta$, where $\Delta\theta \sim 10^{-4}/f_J$. Thus $N >> 10^4$ (for example, for $i \sim i_c$ and $\Gamma \sim 0.05$, $N \sim 10^6$), and the computation of a single spectral density is very time consuming. In addition, many spectral densities (typically 40) must be averaged together to obtain accurate results. We thus use an alternative method to generate v_k; this method significantly reduces the computation time for spectral densities at experimentally relevant values of i and Γ.

Method II. We generate values of the Fourier transform, $\tilde{v}_k$, of the Johnson noise voltages at N equal frequency intervals δf. The interval δf is fixed by the requirement $\delta f << f_J$, and N is fixed by the requirement $N\delta f >> f_J$. The actual values of N and δf are determined empirically by computing low frequency spectral densities S_v^o for the SQUID for variable N and δf. N is increased and δf is decreased until S_v^o becomes independent of N and δf. Typically, N = 512 and $\delta f = 0.01\ f_J$. Our values $\tilde{v}_k$ approximate the Johnson noise in the following way. The Fourier transform of a set of Gaussian distributed noise voltages, v_k, is a set of complex numbers with Gaussian distributed amplitudes and uniformly distributed phases[27]. We approximate the Fourier transform of the noise pulses by a set of complex numbers with constant amplitude and uniformly distributed phases. The amplitude of $\tilde{v}_k$ is fixed by the requirement $\langle v_k^2 \rangle = 2\Gamma N\delta f$, and the random phases are generated by a pseudo-random number generator with uniform distribution over $[0, 2\pi]$. We find that the voltage pulse amplitudes, v_k, generated in this way are Gaussian distributed. Figure 9 shows a histogram of the v_k obtained from 30 sets of $\tilde{v}_k$ in this way, together with the exact Gaussian distribution with $\langle v^2 \rangle = 2\Gamma N\delta f$. The agreement between the two curves is good. This approximation enables us to compute smooth average spectral densities for a single junction using only one set of $\tilde{v}_k$, and for the SQUID using only a small number of sets of $\tilde{v}_k$.

The Fourier transforms of the $\tilde{v}_k$ were taken as representative values of the Johnson noise over pulse times $\delta\theta = 1/2N\delta f$. Since $\delta\theta$ was considerably larger than the value of $\Delta\theta$ used in Method I, we interpolated between adjacent noise values. We found our results for S_v^o were independent

of the details of the interpolation scheme used. Hence we used a linear interpolation for convenience.

We found Methods I and II yielded identical noise-rounded i-$\bar{v}$ characteristics for a single junction (section 4.2). We also computed spectral densities of the voltage noise across a single junction for $i >> i_c$ from $v(\theta)$ generated by Methods I and II. The two methods yielded spectral densities that were in good agreement. However, whereas we needed to average the spectral density typically 40 times using Method I, only a single set of v_k was required using Method II. We also computed spectral densities using $\tilde{v}_k$ with Gaussian distributed amplitudes. The values for S_v^o averaged over many trials were in agreement with those obtained with constant amplitude v_k. We conclude that our approximation scheme adequately represents the Johnson noise for our purposes.

Method II was used to compute the voltage noise spectral densities of the SQUID [Fig. 14]. Equations (2.13)-(2.16) were integrated with interpolated noise values determined by the v_k as in the single junction case. We checked the values of the average voltage computed from $v(\theta)$ at time intervals $\delta\theta$ with those obtained by Method I, and found good agreement. Because the SQUID involves two independent random noise sources, we found it necessary to average S_v^o over typically 8 sets of v_k to achieve a satisfactory result. We estimate that our values of S_v^o are accurate to $\pm$ 5%.

4.2 Single Junction with Noise

In order to test our numerical techniques, we first applied Methods I and II of section 4.1 to the case of a single resistively shunted Josephson junction. For a junction biased at a constant current i, the voltage v and phase δ across the junction satisfy[14]

$$v = i - \sin \delta + v_N \ , \tag{4.1}$$

and $$d\delta/d\theta = v \ , \tag{4.2}$$

where v_N is the Johnson noise voltage across the shunt resistance. We integrated these equations stepwise in time for various values of i and Γ. Representative plots of $\delta(\theta)$ and $v(\theta)$ for $i = 0.9$ and $\Gamma = 0.05$ appear in Fig. 10. The phase $\delta(\theta)$ undergoes random excursions of considerably less than 2π about an equilibrium position for a period of time, then makes a fairly sharp transition of $+ 2\pi$ to an equivalent equilibrium position. These transitions are randomly timed and, according to Eq. (4.2), give rise to voltage pulses during the transitions. These voltage pulses are somewhat obscured in the plot of v vs. θ in Fig. 10(b). The v vs. θ curve appears to be dominated by the random noise source v_N shifted by a constant voltage. This behavior is consistent with Eq. (4.1) since the term $(i - \sin \delta)$ is approximately constant between the transitions $\delta \to \delta + 2\pi$. Notice that, although the excursions of δ around the equilibrium positions are small compared with 2π, the time derivative, $d\delta/d\theta = v$, is not small compared with the amplitude of the voltage pulses associated with the transitions in δ. In fact, as we decrease ΔT to improve our approximation for the Johnson noise source, $v \sim v_N \propto 1/\Delta T$ increases. Since the voltage pulses associated with the 2π transitions of δ have fixed area and duration, they become buried in the Johnson noise voltage pulses as T decreases*.

*Fulton[15] has used a thermal activation model in a simple derivative of

We obtained $i-\bar{v}$ characteristics by time-averaging $v(\theta)$ at fixed i. The $i-\bar{v}$ characteristics obtained using both Methods I and II to generate $v(\theta)$ are shown in Fig. 11(a). The smooth curves are from the Fokker-Planck calculation of Ambegaokar and Halperin.[14] The results of the two numerical techniques are in excellent agreement with each other with the Fokker-Planck calculation.[14] and with other numerical calculations.[13,28]

We also computed voltage power spectral densities, S_v, from curves of v vs. θ using Method II. We observed that the peaks in S_v corresponding to the noise-free Josephson frequency, f_J, and its harmonics become broadened in the presence of thermal noise. As i is reduced, the noise broadening increases in a manner that is consistent with the results of Vystavkin et al.[16] At frequencies well below f_J the power spectrum is white. We take the value of S_v in this region to be the low frequency spectral density S_v^o. In Fig. 11(b) we plot the square root of the normalized low frequency voltage spectral density $(S_v^o/4\Gamma)^{\frac{1}{2}}$ vs. the noise-rounded voltage $\bar{v}$ for two values of Γ. These values are in excellent agreement with the results of Vystavkin et al.[16] (obtained by another method) that are plotted as smooth curves in Fig. 11(b). By comparing Figs. 11(a) and (b), we observe that the maxima in $(d\bar{v}/di)$ and in S_v^o occur at the same value of current,

---

the spectral density of the noise in a resistively shunted junction at currents below i_c. In this model, the noise arises from the random timing of the voltage pulses that occur when δ jumps by 2π. Although according to our calculation these pulses are obscured by the simulated Johnson noise, the results of Fulton's calculation (at low voltage), of the calculation Vystavkin et al.,[16] and of our calculation are all in good agreement.

$i \approx i_c$. In addition, a decrease in the maximum of $d\bar{v}/di$ (for example, as a result of increasing Γ) is accompanied by a decrease in the maximum of S_v^o.

4.3 SQUID Characteristics in the Presence of Noise

4.3.1 SQUID Transfer Function

We now use the methods of section 4.1 to compute from Eqs. (2.13)-(2.16) the voltage $v(\theta)$ and circulating current $j(\theta)$ for the SQUID in the presence of noise. As in section 3.2, we frequently select the value $\beta = 1.0$ in calculating results, since, as we shall see later, this value is optimum for practical SQUIDs. If we choose $\beta = 1.0$ and $L = 1$ nH, we find $I_o \approx 1$ μA and for $T \lesssim 4.2$ K, $\Gamma \lesssim 0.2$. Noise-rounded i-$\bar{v}$ characteristics for the symmetric SQUID are plotted in Fig. 12(a) with $\Gamma = 0.05$ and $\beta = 1.0$ for several values of ϕ_a. The noise-free i-$\bar{v}$ characteristics are also shown. We observe that the differential resistance, $(d\bar{v}/di)$, is a function of both i and ϕ_a. In particular, the maximum differential resistance decreases as ϕ_a increases from 0 to 0.5. From these i-$\bar{v}$ characteristics we obtain the variation of $\bar{v}$ with ϕ_a [Fig. 12(b)] for several values of i with $\Gamma = 0.05$ and $\beta = 1.0$. The corresponding noise-free curves are also shown. For bias currents $i \gtrsim 3$, $\bar{v}$ becomes relatively independent of ϕ_a, while for $i \lesssim 1$, $\bar{v}$ is zero for most values of ϕ_a. At intermediate values of i, the SQUID transfer function, $(\partial\bar{v}/\partial\phi_a)_i$, depends on ϕ_a and the parameters $\beta(L, I_o)$ and $\Gamma(I_o, T)$.

We plot $(\partial\bar{v}/\partial\phi_a)_i$ vs. i for variable ϕ_a, L, T, and I_o in Figs. 13(a)-(d). All the curves show a peak in $(\partial\bar{v}/\partial\phi_a)_i$ at a bias current corresponding roughly to the noise-free critical current determined by ϕ_a and β.

The height and width of the curves are a function of ϕ_a, β, and Γ. For example, the family of curves in Fig. 13(a) for variable ϕ_a ($\Gamma = 0.05$ and $\beta = 1.0$) shows maxima which decrease as $\phi_a \to 0$ and $\phi_a \to 0.5$. At $\phi_a = 0$ and 0.5, $(d\bar{v}/d\phi_a) = 0$ for all values of i. Thus, changes in ϕ_a can produce substantial changes in $(\partial\bar{v}/\partial\phi_a)_i$. The curves of $(\partial\bar{v}/\partial\phi_a)_i$ vs. i for fixed I_o and T, and for variable $L(\propto \beta)$ are plotted in Fig. 13(b) for $\Gamma = 0.05$ and $\phi_a = 0.25$. For $\beta \lesssim 0.1$, the curves approach a limit independent of L. This result reflects the fact that for $\beta \lesssim 0.1$, $\Delta I_c \to 2I_o$ independent of L. For large L ($\beta >> 1$) $(\partial\bar{v}/\partial\phi_a)_i \to 0$.

The temperature dependence of $(\partial\bar{v}/\partial\phi_a)_i$ is plotted in Fig. 13(c) for $\phi_a = 0.25$ and $\beta = 1.0$. As T ($\propto \Gamma$) increases, the SQUID i-$\bar{v}$ characteristics approach the i-$\bar{v}$ characteristics of the shunts, and hence $(\partial\bar{v}/\partial\phi_a)_i \to 0$. For $T \to 0$ ($\Gamma \lesssim 0.001$), the SQUID i-$\bar{v}$ characteristics approach the noise-free curves. Thus $(\partial\bar{v}/\partial\phi_a)_i$ approaches a noise-free limit that diverges at $i = i_c(\beta, \phi_a)$.

The critical current I_o appears in both the parameters β ($\propto I_o$) and Γ ($\propto 1/I_o$). Thus, in Fig. 13(d), the curves of $(\partial\bar{v}/\partial\phi_a)_i$ vs. i for variable I_o reflect a combination of Figs. 13(b) and (c). Since the dependences of $(\partial\bar{v}/\partial\phi_a)_i$ on β and Γ tend to cancel as I_o is varied, $(\partial\bar{v}/\partial\phi_a)$ is less strongly dependent on I_o than on β or Γ separately*. In the limit of large I_o ($\Gamma << 0.1$, $\beta >> 10$) the values of $(\partial\bar{v}/\partial\phi_a)_i$ approach the noise-free large β limit, and $(\partial\bar{v}/\partial\phi_a)_i \to 0$ for all i. This result is consistent with the fact that as $\beta \to \infty$, $\Delta I_c \to \Phi/L$ [Fig. 4(b)],

*Notice that $(\partial\bar{v}/\partial\phi_a)_i$ is a dimensionless quantity. The corresponding dimensional variable $(I_oR/\phi_o)(\partial\bar{v}/\partial\phi_a)_i$ is roughly proportional to I_o for the range of parameters in Fig. 13(d).

or $\Delta i_c = \Delta I_c / I_o \rightarrow \Phi_o / L I_o = 2/\beta$. Hence the i-$\bar{v}$ curves for all i and ϕ_a collapse into the $\phi_a = 0$ curve as $\beta \rightarrow \infty$, and $(\partial \bar{v}/\partial \phi_a)_i \rightarrow 0$. Although in the range displayed in Fig. 13(d) $(\partial \bar{v}/\partial \phi_a)_i$ increases as I_o decreases, in fact, for very low values of I_o, $(\partial \bar{v}/\partial \phi_a)_i$ must fall off, and tend to zero as $I_o \rightarrow 0$. This behavior is a result of the fact that when $\beta \rightarrow 0$, $(\partial \bar{v}/\partial \phi_a)_i \rightarrow$ constant [Fig. 13(b)], whereas when $\Gamma \rightarrow \infty$, $(\partial \bar{v}/\partial \phi_a)_i \rightarrow 0$ [Fig. 13(c)].

4.3.2 SQUID Voltage Noise

We computed voltage spectral densities for the SQUID as a function of the various parameters using Method II of section 4.1. The spectral densities have the same general characteristics as the spectral densities of the single junction. There are a series of noise braodened peaks at the Josephson frequency, f_J, and harmonics. Well below f_J the spectral density is white; we are interested in S_v^o, the average value of the spectral density in this low frequency range.

In Fig. 14(a), we plot the normalized frequency voltage spectral density $S_v^o/2\Gamma$ vs. i for $\beta = 1.0$ and $\Gamma = 0.05$ for four values of ϕ_a. For $i >> i_c(\phi_a)$ the spectral densities approach the Johnson noise limit of 1.0 (for two shunts in parallel, the shunt spectral density is 2Γ). Near $i_c(\phi_a)$, the spectral density is a maximum, as in the case of the single junction. The value of the maximum decreases as ϕ_a increases from 0 to 0.5. This effect is consistent with the decrease in the maximum differential resistance, $(d\bar{v}/di)$, with increasing flux that is observed in the noise rounded i-$\bar{v}$ characteristics (sec. 4.3.1).

The dependence of $S_v^o/2\Gamma$ on the variables L, T, and I_o for $\phi_a = 0.25$ is plotted in Figs. 14(b)-(d). As the inductance L ($\propto \beta$) increases [Fig. 14(b)],

$S_v^o/2\Gamma$ approaches the limit of a single junction with critical current $2I_o$. In the low inductance limit ($\beta \lesssim 0.1$), the spectral densities approach a limiting form. This result is consistent with the independence of ΔI_c [Fig. 4(a)] and $(\partial\bar{v}/\partial\phi_a)_i$ [Fig. 13(b)] on L in the low β limit.

The dependence of $S_v^o/2\Gamma$ on temperature [Fig. 14(c)] is similar to that of the single junction. As $T \to 0$ ($\Gamma \lesssim 0.01$), the spectral density approaches a limit determined by the noise-free differential resistance; as $i \to i_c$, $(\partial\bar{v}/\partial i)_{\phi_a} \to \infty$, and $S_v^o/2\Gamma$ diverges. In the large temperature limit ($\Gamma \gtrsim 1$) the noise tends to the Johnson noise of the shunts, and $S_v^o/2\Gamma \to 1$ for all i.

The dependence of $S_v^o/2\Gamma$ on I_o [Fig. 14(d)] is a combination of the effects in Figs. 14(b) and (c). In the limit $I_o \to \infty$ ($\beta \to \infty$, $\Gamma \to 0$), the curves approach the corresponding single junction noise-free limit. As $I_o \to 0$ ($\beta \to 0$, $\Gamma \to \infty$), the β-dependence drops out for $\beta \lesssim 0.1$, and the curves approach the Johnson noise limit, $S_v^o/2\Gamma = 1$.

4.3.3 SQUID Flux Noise

We take as a measure of the rms flux noise the dimensionless ratio $\zeta_\phi^{1/2} = (S_v^o/2\Gamma)^{1/2}/(\partial\bar{v}/\partial\phi_a)_i$. Curves of $\zeta_\phi^{1/2}$ vs. i for variable ϕ_a, L, T, and I_o are plotted in Figs. 15(a)-(d). The family of curves for variable ϕ_a with $\Gamma = 0.05$ and $\beta = 1.0$ [Fig. 15(a)] exhibit minima at $i \sim i_c(\phi_a)$. For $0.1 < \phi_a < 0.4$, the value of $\zeta_{\phi\,\min}^{1/2}$ is relatively independent of ϕ_a for $\beta = 1.0$, $\Gamma = 0.05$. For $\phi_a \to \pm n/2$ ($n = 0, 1, 2, \ldots$), $\zeta_\phi^{1/2} \to \infty$ for all values of $i[(\partial\bar{v}/\partial\phi_a)_i \to 0)]$.

The family of curves of $\zeta_\phi^{1/2}$ vs. i for variable L ($\propto \beta$) [Fig. 15(b)] with $\Gamma = 0.05$ and $\phi_a = 0.25$ also have minima at $i \sim i_c(\beta)$. As $\beta \to 0$

the curves become progressively flatter, and $\zeta_{\phi}^{\frac{1}{2}}{}_{\min}$ approaches a limit ≈ 0.5. As β increases beyond unity, the curves become sharper with $\zeta_{\phi}^{\frac{1}{2}}{}_{\min}$ growing roughly as β.

The dependence of $\zeta_{\phi}^{\frac{1}{2}}$ on temperature [Fig. 15(c)] is weak for $0.025 < \Gamma < 0.075$, where $\zeta_{\phi} \approx 1.0$. In the high temperature limit ($T \propto \Gamma \to \infty$), $S_v^o/2\Gamma \to 1$ and $(\partial\bar{v}/\partial\phi_a)_i \to 0$; hence we expect $\zeta_{\phi}^{\frac{1}{2}} \to \infty$. For $\Gamma \propto T \to 0$, both $S_v^o/2\Gamma$ and $(\partial\bar{v}/\partial\phi_a)_i$ diverge at $i = i_c(\beta, \phi_a)$; $\zeta_{\phi}^{\frac{1}{2}}$ becomes a sharp function of i, falling to zero as $i \to i_c$.

A family of curves of $\zeta_{\phi}^{\frac{1}{2}}$ for variable I_o is plotted in Fig. 15(d) for $\phi_a = 0.25$. As I_o increases, the curves of $\zeta_{\phi}^{\frac{1}{2}}$ become progressively sharper, and $\zeta_{\phi}^{\frac{1}{2}}{}_{\min}$ increases. As I_o decreases, the curves flatten for intermediate values of β; however, for very small values of I_o, the dependence of $\zeta_{\phi}^{\frac{1}{2}}$ on β drops out, and $\zeta_{\phi}^{\frac{1}{2}} \to \infty$ as $\Gamma \to \infty$.

4.4 SQUID Energy Resolution

In this section we relate the computed flux noise spectral density, ζ_{ϕ}, to the energy resolution of the SQUID, $S_{\Phi}/2L$. We compare our results with high-and-low-β limiting expressions and with experimental results.

We take the flux noise referred to the output of the SQUID as $S_{\Phi}^o = S_V^o/(\partial\bar{v}/\partial\Phi_a)_I^2$. With $(\partial\bar{v}/\partial\Phi_a)_I = (\partial\bar{v}/\partial\phi_a)_i I_o R/\Phi_o$, $S_V^o = (S_V^o/2\Gamma)2k_BTR$, and $2L = \beta\Phi_o/I_o$, we have the following expression for $S_{\Phi}^o/2L$ in terms of ζ_{ϕ}:

$$S_{\Phi}^o/2L = (\Phi_o^2/\pi)\,\zeta_{\phi}(\beta, \Gamma, i, \phi_a)\,\Gamma/R\beta\ , \tag{4.3}$$

$$\text{or}\quad S_{\Phi}^o/2L = (2k_BTL/R)\,(2/\beta^2)\,\zeta_{\phi}(\beta, \Gamma, i, \phi_a)\ . \tag{4.4}$$

Equations (4.3) and (4.4) are exact expressions for the energy resolution in terms of the computed flux spectral density, ζ_{ϕ}.

From a different viewpoint, we can derive approximate expressions for the energy resolution in the high- and low-β limits as follows[2,3]. For $\Phi \approx (n \pm \frac{1}{4})\Phi_o$, we take $(\partial\bar{V}/\partial\Phi_a)_I \approx (\partial\bar{V}/\partial I_c)_I (dI_c/d\Phi_a) \approx R\Delta I_c/\Phi_o$, where we have set $(\partial\bar{V}/\partial I_c)_I \approx (R/2)$ for $I \approx I_c$, and $dI_c/d\Phi_a = 2\Delta I_c/\Phi_o$. From Fig. 4(b), we find $\Delta I_c \approx \Phi_o/L$ for $\beta \gtrsim 40$, so that $(\partial V/\partial\Phi_a)_I \approx R/L$ as $\beta \to \infty$. From Fig. 4(a), we find that for $\beta \lesssim 0.1$, $\Delta I_c \approx 2I_o \approx \beta\Phi_o/L$, and $(\partial\bar{V}/\partial\Phi_a)_I \approx \beta R/L$. We make the following approximation[2] for S_V^o. For $I_o = 0$ (shunt resistances only), the voltage spectral density is $S_V^R = 4k_BT(R/2)$ and the circulating current spectral density is $S_J^R = 4k_BT/(2R)$, where S_V^R and S_J^R are independent and uncorrelated. For the SQUID ($I_o \neq 0$), the voltage is a function of the currents flowing through the junctions and around the SQUID loop. Hence S_V and S_J are no longer uncorrelated, and $S_V^o > S_V^R$ for $I \sim I_c$. The contribution of the circulating currents to S_V^o is approximated by $(\partial\bar{V}/\partial\Phi_a)_I^2 S_\Phi^R$, where $S_\Phi^R = L^2 S_J^R$. Thus

$$S_V^o \simeq S_V^R + (\partial\bar{V}/\partial\Phi_a)_I^2 L^2 S_J^R . \tag{4.5}$$

In the high β limit, $(\partial\bar{V}/\partial\Phi_a)_I \approx R/L$, and

$$S_\Phi^o/2L \approx 2k_BTL/R, \quad (\beta >> 1), \tag{4.6}$$

while in the low β limit, $(\partial V/\partial\Phi_a)_I \approx R/\beta L$ and

$$S_\Phi^o/2L \approx k_BTL/R\beta^2, \quad (\beta << 1) . \tag{4.7}$$

We now compare the computed expression for S_Φ [Eq. (4.4)] with the approximate expressions [Eqs. (4.6) and (4.7)]. In the high β-limit, our calculated curves of $\zeta_\phi^{\frac{1}{2}}$ vs. i become sharp functions of i. We choose the minimum value of $\zeta_\phi^{\frac{1}{2}}$ corresponding to $i \approx i_c(\phi_a, \beta)$ for the comparison. Calculations of ζ_ϕ for $\phi_a = 0.25$ and $\beta \gtrsim 10$ yield $\zeta_\phi \approx \beta^2/2$ at $i \sim i_c(\phi_o, \beta)$, and hence $S_\Phi^o/2L \approx 2k_BTL/R$, in agreement with Eq. (4.6). From Fig. 15(b), for $\Gamma = 0.05$ and $\phi_a = 0.25$, we see that $\zeta_\phi^{\frac{1}{2}}$ approaches a limit of about 0.5

for $\beta \lesssim 0.1$ over a wide range of bias currents. Hence, from Eq. (4.4), $S_\Phi^o/2L \to k_B TL/R\beta^2$ as $\beta \to 0$, in agreement with Eq. (4.7). We conclude that Eq. (4.4) shows the correct limiting behavior for high and low β.

Finally, we compared our computed results with the measured flux resolution of the tunnel junction dc SQUID of Clarke et al.[2] It should be noted that whereas the model calculation assumes that the junction capacitance is zero, practical junctions have a capacitance and are usually operated with $\beta_c = 2\pi I_c R^2 C/\Phi_o \approx 1$. However, since the I-V characteristics with $\beta_c = 1$ are not very different from those with $\beta_c = 0$,[18] and since we are concerned with frequencies much less than $(RC)^{-1}$, we do not expect the calculated flux noise power spectra with $\beta_c = 1$ to differ substantially from our calculated spectra.

In the tunnel junction SQUID, the inductance was L = 1 nH, the shunt resistance was R = 0.6 Ω, and the critical current of each junction, was about 2.5 μA. Thus $\beta \approx 2.5$ and $\Gamma \approx 0.072$. The SQUID was biased above the critical current at $i \sim 2$, and a modulating flux of peak amplitude $\phi_o/4$ was applied. The ac voltage across the SQUID was demodulated with a lock-in amplifier, and the output from the lock-in was fed back to flux-lock the SQUID in the usual manner. The measured flux resolution was $S_\Phi^{1/2} \approx 3.5 \times 10^{-5}\ \Phi_o\ \mathrm{Hz}^{-1/2}$. We compute a flux resolution for the SQUID with Φ_a fixed at $\Phi_o/4$ of $S_\Phi^{1/2} = 1.3 \times 10^{-5} \Phi_o/\sqrt{\mathrm{Hz}}$. This value applies to a SQUID that is not flux modulated, but is used as a small signal amplifier for Φ_a near $\Phi_o/4$. The flux modulation scheme increases $S_\Phi^{1/2}$ as follows. First, the voltage noise S_V^o of the SQUID is a function of the modulation flux. For a SQUID biased at i = 2 and modulated about $\phi_a = 0$, we estimate that the effective modulated voltage noise is $S_{V_m}^o \lesssim 2\ S_V^o\ (\phi_a = 0.25)$ [see

Fig. 15(a)]. Second, the transfer function $(\partial\bar{V}/\partial\Phi_a)_I$ at $\Phi_q = \Phi_o/4$ must be replaced with $(\partial V_m/\partial\Phi_q)_I$ at $\Phi_q = 0$, where V_m is the amplitude of the Fourier component of the SQUID voltage at the modulation frequency, $\omega_o/2\pi$, and Φ_q is the quasistatic applied flux. By plotting $\bar{V}$ vs. t for $\Phi_a = \Phi_q + (\Phi_o/4) \cos \omega_o t$ from the curves of $\bar{V}$ vs. Φ_a [Fig. 12(b)], we find $(\partial V_m/\partial\Phi_q)_I$ at $\Phi_q = 0$ is approximately equal to $1.3(\partial\bar{V}/\partial\Phi_a)_I$ at $\Phi_a = \Phi_o/4$. From these results, we compute a flux resolution for the modulated SQUID of $S_\Phi^{\frac{1}{2}} \approx 1.6 \times 10^{-5} \Phi_o \mathrm{Hz}^{-\frac{1}{2}}$. In view of the uncertainty in the measured values of the SQUID parameters and of the neglect of the capacitance in the calculation, we conclude that the computed spectral density of the flux noise is in sensible agreement with the experimentally measured value.

5. SQUID OPTIMIZATION

We now consider the choice of the SQUID parameters L, R, I_o, and the bias current i that minimizes the energy resolution at a given temperature T. In most practical applications the SQUID is coupled to a signal coil with coupling coefficient α, and, for magnetometers and voltmeters, the appropriate low frequency figure of merit[2] is $S_\Phi^o/2\alpha^2L$. Since $S_\Phi^o \propto L^2$ in the high β limit [Eq. (4.6)], the figure of merit can be reduced by decreasing L, provided that α^2 is not also correspondingly decreased. In practice, the constraint on α^2 appears to impose a lower limit on L of 10^{-10} to 10^{-9} H. To avoid hysteresis, the junction parameters must also satisfy the constraint $2\pi I_o R^2 C \lesssim \Phi_o$, where C is the junction capacitance. In practice, there is a lower limit on C that is set by the area of the smallest tunnel junction that can be fabricated. Hence, there is an upper limit on R for fixed I_o of $R^2 \lesssim \Phi_o/2\pi I_o C$. Thus for L and C fixed, $S_\Phi^o/2\alpha^2L$ becomes a function only of I_o and T, or of $\beta = I_o(2L/\Phi_o)$ and $\Gamma = 2\pi k_B T/I_o\Phi_o$.

We consider first the simpler case in which the SQUID is not in a flux-locked loop, but is operated as a small signal amplifier with no ac flux modulation. We assume that α is essentially independent of L. From Eqs. (4.6) and (4.7) we find $S_\Phi^o/2L \propto \beta^{\frac{1}{2}}$ ($\beta \gg 1$) and $S_\Phi^o/2L \propto \beta^{-3/2}$ ($\beta \ll 1$). Consequently, there is an intermediate value of β that minimizes $S_\Phi^o/2L$. As an example, consider a cylindrical tunnel junction SQUID in which the diameter of the cylinder is reduced to 2 mm, and the area of the junctions is reduced to 10^{-6} mm^2. The appropriate parameters are estimated to be L = 0.35 nH, C = 1 pF, R^2I_o = 200 Ω^2 μA ($2\pi I_o R^2 C/\Phi_o \approx 0.6$),

and T = 4.2 K. In Fig. 16 we plot computed values of $S_\Phi^o/2L$ vs β with $i = i_c(\phi_a, \beta)$, and $\phi_a = 0.25$. Equations (4.6) and (4.7) are also plotted for all values of β: Notice that the computed value of $S_\Phi^o/2L$ agrees well with these equations in the appropriate limits. The computed curve is almost constant for $1 \lesssim \beta \lesssim 10$. A SQUID operated as a small signal amplifier with $\alpha \approx 1$ at $\Phi_a = 0.25$ and $i = i_c(\phi_a, \beta)$ would have an energy resolution of about 1.6×10^{-32} JHz^{-1} relatively independent of β in that range.

When the SQUID is flux modulated and operated in the usual flux-locked mode, the energy resolution depends more strongly on β than in the unmodulated case. Since the optimal choice of bias current depends on the applied flux, the SQUID operated at constant bias current cannot be optimally biased over the entire modulation cycle. As a result, as β increases the average value of $S_\Phi^o/2L$ at fixed bias current also increases. In addition, from Fig. 15 we see that $S_\Phi^o/2L$ becomes a sharp function of $i = I/I_o$ for large β. Thus small variations in the bias current I or the junction critical current I_o can lead to substantial increases in $S_\Phi^o/2L$. Hence, for the flux modulated SQUID with L = 0.35 nH, C = 1 pF, $R^2I_o = 200\ \Omega^2\mu$A and T = 4.2 K, the optimal value of β is approximately 1. Similar calculations at other values of the SQUID parameters also lead to $\beta \approx 1$ as the value for optimal energy resolution in the flux-locked mode. We estimate an energy resolution of 1.9×10^{-32} JHz^{-1} for the flux-locked SQUID from an analysis similar to that in Sec. (4.4).

In summary, the procedure to obtain optimum performance from a tunnel junction SQUID is as follows. One first chooses a SQUID configuration,

and thus one fixes L. The critical currents of the junctions are set by the constraint $\beta = 2\,LI_o/\phi_o \approx 1$. The shunt resistance, R, for each junction is chosen to satisfy $2\,\pi I_o R^2 C/\Phi_o \lesssim 1$, where C is determined by the area of the junction. Finally, the SQUID is operated with a bias current approximately equal to the total critical current in the absence of noise.

6. ULTIMATE PERFORMANCE OF THE DC SQUID

The dependence of $S_\Phi^o/2L$ on L, C, and T for $\beta = 1$ can be approximated as follows. From Fig. 15 we find $\zeta_\phi^{\frac{1}{2}}(\beta, \Gamma) \approx 1$ for $\beta = 1$. Hence, from Eq. (4.4), we find $S_\Phi^o/2L \approx 4k_BTL/R$ or

$$S_\Phi^o/2L \approx 4k_BT(\pi LC)^{\frac{1}{2}} \qquad (\beta = 1), \tag{6.1}$$

where we have used the constraint $R^2 = \Phi_o/2\pi I_o C = L/\pi C$. Thus, apart from numerical factors close to unity, the energy resolution for $\beta = 1$ is just k_BT divided by the resonant frequency of the ring, $1/2\pi(LC/2)^{\frac{1}{2}}$. We expect Eq. (6.1) to remain valid provided the Johnson noise associated with the shunts is the dominant noise source. However, when $k_BT/eV \approx k_BT/I_oR \lesssim 1$ (V is the bias voltage), the shot noise in the tunnel junctions will be the dominant noise source.[24] For junctions biased at a current of about $2I_o$, the shot noise voltage will have a low frequency spectral density of approximately $2e(2I_o)(R/2)^2 \approx eI_oR^2$ in the low temperature limit. If we replace $2k_BTR$ with eI_oR^2 in Eqs. (4.6) and (4.7), we obtain

$$S_\Phi^o/2L \approx h\beta/4 \qquad (\beta >> 1,\ eI_oR >> k_BT), \tag{6.2}$$

$$\text{and} \quad S_\Phi^o/2L \approx h/8\beta \qquad (\beta << 1,\ eI_oR >> k_BT). \tag{6.3}$$

For the optimum value $\beta \approx 1$, Eq. (6.1) becomes

$$S_\Phi^o/2L \approx h/2 \qquad (\beta = 1,\ eI_oR >> k_BT)\ . \tag{6.4}$$

Thus, it appears possible to operate a SQUID with its energy resolution limited by the uncertainty principle. With $\beta = 1$, this limit requires $4k_BT(\pi LC)^{\frac{1}{2}} \lesssim h/2$. If we choose T = 4.2 K, and L = 0.35 nH, this inequality implies $C \lesssim 10^{-2}$ pF, or a junction area $\lesssim 10^{-11}$ mm^2 for Nb-NbOx-Pb junctions.[29] In principle, junctions of these dimensions can be fabri-

cated with electron beam milling techniques. For $\beta \approx 1$ and L = 0.35 nH, the required critical current, $I_o \approx 3$ μA, corresponds to a current density of about 3 kA cm^{-2}, a value that is readily achieved with junctions of larger area.[29] The shunt resistance is about 100 Ω. These values of L and C correspond to a SQUID frequency, $1/2\pi(LC/2)^{\frac{1}{2}}$, of approximately 10^{11} Hz. Although this frequency is below the gap frequency ($\sim 3 \times 10^{11}$ Hz), other relaxation processes may limit the SQUID to a lower frequency of operation. In that case, it will not be possible to achieve the resolution given by Eq. (5.4) with a SQUID operated at 4.2 K.

One may also attempt to achieve the resolution suggested by Eq. (6.4) by operating the SQUID at a lower temperature: With L = 0.35 nH and C = 1 pF, the temperature must be below 0.4 K. The corresponding frequency at which the SQUID would operate is about 10^{10} Hz. A preamplifier with a noise temperature below 0.4 K would be required.

APPENDIX A

We derive the response of the SQUID shown in Fig. 1(b) to a signal current I_S applied to one superconducting arm of the SQUID. The current I_S generates a current $I_S/2$ in the inductances L_1 and L_2 and in L_3 and L_4, together with a circulating current J_S. These currents are superimposed on the currents I/2 and J produced by the bias current, I. Hence the currents through L_1, L_2, L_3, and L_4 are

$$I_1 = I/2 - J - I_S/2 - J_S \ , \tag{A1}$$

$$I_2 = I/2 + J + I_S/2 + J_S \ , \tag{A2}$$

$$I_3 = I/2 - J + I_S/2 - J_S \ , \tag{A3}$$

and $$I_4 = I/2 + J - I_S/2 + J_S \ . \tag{A4}$$

The bias current I is constant in time; we assume that I_S is quasistatic Thus, $dI_1/dt = dI_3/dt = - dI_4/dt = - dI_2/dt = - dJ_T/dt$, where $J_T = J + J_S$.

Since only the time dependent circulating currents J and J_S determine the voltages across the inductances, Eqs. (2.11) and (2.12) become

$$V = V_1 - (1 - \eta)(L/2)(dJ_T/dt) \ , \tag{A5}$$

and $$V = V_2 + (1 + \eta)(L/2)(dJ_T/dt) \ . \tag{A6}$$

As in sec. 2, the parameter η describes the imbalance between the inductance of the arm containing L_1 and L_3, and the arm containing L_2 and L_4. Equations (2.3)-(2.6) for V_1, V_2, δ_1, and δ_2 are unchanged. Equation (2.10) for the total flux Φ_T is modified by I_S. We define a parameter ξ analogous

to η that describes the imbalance between the inductance of the arm containing L_1 and L_2, and the arm containing L_3 and L_4; the signal flux is then $\Phi_s = LJ_s + \xi LI_s/2$. Hence

$$\Phi_T = LJ_T + \eta LI/2 + \xi LI_s/2 \ . \tag{A7}$$

From Eqs. (A1)-(A7) with Eqs. (2.3)-(2.6), the basic equations in dimensionless parameters are:

$$j_T = (\delta_1 - \delta_2)/\pi\beta - \eta i/2 - \xi i_s/2 \ , \tag{A8}$$

$$v = \frac{(1 + \eta)}{2} \frac{d\delta_1}{d\theta} + \frac{(1 - \eta)}{2} \frac{d\delta_2}{d\theta} \ , \tag{A9}$$

$$\frac{d\delta_1}{d\theta} = \frac{i/2 - (i_s/2 + j_T) - (1 - \alpha) \sin \delta_1}{(1 - \rho)} + v_{N1} \ , \tag{A10}$$

$$\frac{d\delta_2}{d\theta} = \frac{i/2 + (i_s/2 + j_T) - (1 + \alpha) \sin \delta_2}{(1 + \rho)} + v_{N2} \ . \tag{A11}$$

Equations (A8)-(A11) have the same form as Eqs. (2.13)-(2.16) if we identify j with $(j_T + i_s/2)$ and ϕ_a with $-(1 - \xi)\beta\, i_s/4$.

APPENDIX B

The procedure used to calculate $i_c(\phi_a)$ is as follows. By combining Eqs. (3.1)-(3.3) we eliminate j, and express δ_2 as a function of δ_1 and i:

$$\delta_2 = \delta_1 - 2\pi\phi_a - \pi\beta i(1 + \eta)/2 + \pi\beta(1 - \eta)\ \sin\delta_1 . \qquad (B1)$$

We define a function of i and δ_1 to be

$$F(i,\delta_1) = i - (1 - \alpha)\ \sin\delta_1 - (1 + \alpha)\ \sin\delta_2 . \qquad (B2)$$

Eq. (3.1) is satisfied when $F(i,\delta_1) = 0$. Plots of $F(i,\delta_1)$ vs. δ_1 for fixed i generate a family of continuous curves each labeled by the value of i. Since F is also continuous in i, the curve corresponding to the greatest value of i that still has a zero (i.e. $F(i,\delta_1) = 0$ for some δ_1) will necessarily satisfy $\partial F/\partial\delta_1 = 0$ at that point. Hence,

$$\partial F/\partial\delta_1 = -(1 - \alpha)\ \cos\delta_1 - (1 + \alpha)[1 + \pi\beta(1 - \alpha)\ \cos\delta_1]\ \cos\delta_2 . \qquad (B3)$$

Equation (B2) with F = 0 and Eq. (B3) with $\partial F/\partial\delta_1 = 0$ allow us to express δ_1 in terms of i:

$$i = (1 - \alpha)\ \sin\delta_1 + \left\{(1 + \alpha)^2 - \left[\frac{(1 - \alpha)\ \cos\delta_1}{1 + \pi\beta(1 - \alpha)\ \cos\delta_1}\right]^2\right\}^{1/2} . \qquad (B4)$$

Now both F and $\partial F/\partial\delta_1$ can be expressed as function of a single variable δ_1. We search for the simultaneous zeros of F and $\partial F/\partial\delta_1$ with respect to δ_1 using a Newton-Raphson search routine in one variable only, and thus determine the maximum supercurrent, i_c, as a function of α, β, η, and ϕ_a.

APPENDIX C

We show that $\phi_a^\eta = \phi_a^o - \beta\eta i/4$. Suppose the set of values (v^o, j^o, ϕ_a^o) satisfy Eqs. (2.13)-(2.16) for arbitrary α, ρ, β, and i with $\eta = 0$. We want to show that the set $(v^\eta, j^\eta, \phi_a^\eta)$ for $\eta \neq 0$ can be shifted so that the shifted values satisfy the $\eta = 0$ equations, and hence have the $\eta = 0$ time-averaged values. Now the set $(v^\eta, j^\eta, \phi_a^\eta)$ satisfy Eqs. (2.13)-(2.16) with $\eta \neq 0$. Rewriting these equations, we have

$$j^\eta = (\delta_1 - \delta_2)/\pi\beta - (\phi_a^\eta - \pi\beta i/4)2/\beta \ ,$$

$$\text{and } v^\eta - (d\delta_1/d\theta - d\delta_2/d\theta)\eta/2 = (d\delta_1/d\theta + d\delta_2/d\theta)/2 \ .$$

Since both ϕ_a and i are independent of time, we have

$$\eta\beta dj^\eta/d\theta = d\delta_1/d\theta - d\delta_2/d\theta \ .$$

Hence

$$v^\eta - (\pi\eta\beta/2)dj^\eta/d\theta = (d\delta_1/d\theta + d\delta_2/d\theta)/2 \ .$$

If we take $v^s = v^\eta - (\pi\eta\beta/2)dj^\eta/d\theta$, $j^s = j^\eta$, and $\phi_a^s = \phi_a^\eta - \pi\beta i/4$ we see that the shifted set (v^s, j^s, ϕ_a^s) satisfy Eqs. (2.13)-(2.16) for $\eta = 0$. Hence the time-averaged values $\overline{v^s}$ and $\overline{j^s}$ evaluated at ϕ_a^s will equal the original average values $\overline{v^o}$ and $\overline{j^o}$ at $\phi_a^o = \phi_a^s$. But $\overline{j^s} = \overline{j^\eta}$, and $\overline{v^s} = \overline{v^\eta} - (\pi\eta\beta/2)dj^\eta/dt = \overline{v^\eta}$. Hence the values $\overline{v^\eta}$ and $\overline{j^\eta}$ at some ϕ_a^η are just the values of $\overline{v^o}$ and $\overline{j^o}$ at $\phi_a^\eta - \eta\beta i/4$. Consequently, an imbalance η in the SQUID inductance appears as an effective external flux $- \eta\beta i/4$ for fixed bias current i.

References

1. R. C. Jaklevic, J. Lambe, A. H. Silver, and J. E. Mercereau, Phys. Rev. Lett. 12, 159 (1964); Phys. Rev. Lett. 14, 887 (1965); Phys. Rev. 140, A1628 (1965).
2. J. Clarke, W. M. Goubau, and M. B. Ketchen, J. Low Temp. Phys. 25, 99 (1976).
3. M. Tinkham, Introduction to Superconductivity (McGraw-Hill, 1975), p. 214.
4. J. E. Zimmerman and A. H. Silver, Phys. Rev. 141, 367 (1966).
5. E. O. Schulz-DuBois, IBM Research RZ 564, April 13, 1973.
6. A. Th. A. M. De Waele and R. De Bruyn Ouboter, Physica 41, 225 (1969).
7. A. Th. A. M. De Waele and R. De Bruyn Ouboter, Physica 42, 626 (1969).
8. T. A. Fulton, Solid State Commun. 8, 1353 (1970).
9. J. Clarke and J. L. Paterson, Appl. Phys. Lett. 19, 469 (1971).
10. W.-T. Tsang and T. Van Duzer, J. Appl. Phys. 46, 4573 (1975).
11. T. A. Fulton, L. N. Dunkleberger, and R. C. Dynes, Phys. Rev. B6, 855 (1972).
12. W.-T. Tsang and T. Van Duzer, J. Appl. Phys. 47, 2656 (1976).
13. F. Auracher, Ph.D. thesis, University of California, Berkeley (1973).
14. V. Ambegaokar and B. I. Halperin, Phys. Rev. Lett. 22, 1364 (1969).
15. T. A. Fulton, IEEE Trans. Magn. MAG-11, 749 (1975).
16. A. N. Vystavkin, V. N. Gubankov, L. S. Kuzmin, K. K. Likharev, V. V. Migulin, and V. K. Semenov, Rev. Phys. Appl. 9, 79 (1974).
17. C. Tesche and J. Clarke, IEEE Trans. Magn. MAG-13, 859 (1977).
18. W. C. Stewart, Appl. Phys. Lett. 12, 277 (1968); D. E. McCumber, J. Appl. Phys. 39, 3113 (1968).
19. J. Clarke, Phil. Mag. 13, 115 (1966).

20. M. B. Ketchen, W. M. Goubau, J. Clarke, and G. B. Donaldson, IEEE Trans. Magn. MAG-13, 372 (1977).

21. L. Solymar, Superconductive Tunneling and Applications (Chapman and Hall, London, 1972), p. 202.

22. J. Clarke and J. L. Paterson (unpublished).

23. L. G. Aslamazov, A. I. Larkin, and Yu.N. Orchinnikov, JETP 28, 171 (1969).

24. A. J. Dahm, A. Denenstein, D. N. Langenberg, W. H. Parker, D. Rogovin, and D. J. Scalapino, Phys. Rev. Lett. 22, 1416 (1969).

25. M. J. Stephen, Phys. Rev. Lett. 21, 1629 (1968).

26. G. A. Hawkins and J. Clarke, J. Appl. Phys. 47, 1616 (1976).

27. A. Van der Ziel, Noise (Prentice-Hall, Inc., New York, 1954), p. 320.

28. J. Kadlec and K. H. Gundlach (preprint).

29. S. Basavaiah and J. H. Greiner, J. Appl. Phys. 47, 4201 (1976).

Figure Captions

Fig. 1 Model for the dc SQUID with (a) externally applied flux Φ_a, and (b) flux generated by a current, I_s

Fig. 2 Critical current of SQUID vs. applied flux as a function of (a) α, and (b) η.

Fig. 3 Critical current of SQUID vs. applied flux as a function of β.

Fig. 4 Critical current modulation vs. β as a function of (a) L, and (b) I_o.

Fig. 5 Voltage and circulating current vs. time as functions of applied flux, α, η, and ρ.

Fig. 6 Current-voltage characteristics of symmetric SQUID as a function of (a) applied flux, and (b) β.

Fig. 7 (a) Average voltage and (b) average circulating current vs. applied flux as a function of β.

Fig. 8 (a), (d), (g) Current-voltage characteristics; (b), (e), (h) average circulating current vs. applied flux; and (c), (f), (i) average voltage vs. applied flux, for SQUID as functions of η, α, and ρ. In all cases $\beta = 1$.

Fig. 9 Histogram of random voltages v_k generated by Method II for 30 trials. Dotted curve is Gaussian with the same normalization.

Fig. 10 Representative plots of (a) phase, and (b) associated voltage vs. time for single junction with $\Gamma = 0.05$, and $i = 0.9$.

Fig. 11 (a) Current-voltage characteristics of single resistively shunted junction in presence of noise computed with Method I (•), and Method II (Δ, $\square$, o). Solid curves are from Ambegaokar and

Halperin.[14] Dotted line is noise-free characteristic. (b) Low frequency voltage spectal density vs. average voltage for single resistively shunted junction computed with Method II (Δ, □, o). Solid curves are from Vystavkin et al.[16]

Fig. 12 (a) Current-voltage characteristics of SQUID in presence of noise as functions of applied flux computed with Method I (•), and Method II (Δ, □, o). Dotted lines are noise-free characteristics. (b) Average voltage vs. applied flux for SQUID as function of bias current, i, in presence of noise with $\Gamma = 0.05$ (solid lines). Dotted lines are noise-free values.

Fig. 13 SQUID transfer function vs. bias current as a function of (a) applied flux, (b) SQUID inductance, (c) temperature, and (d) critical current per junction.

Fig. 14 Low frequency voltage spectral density vs. bias current as a function of (a) applied flux, (b) SQUID inductance, (c) temperature, and (d) critical current per junction. Dashed lines represent Johnson noise limit.

Fig. 15 Flux noise spectral density, $\zeta_\phi^{1/2}$, vs. bias current i as a function of (a) applied flux, (b) SQUID inductance, (c) temperature, and (d) critical current per junction.

Fig. 16 $S_\Phi^o/2L$ vs. β.

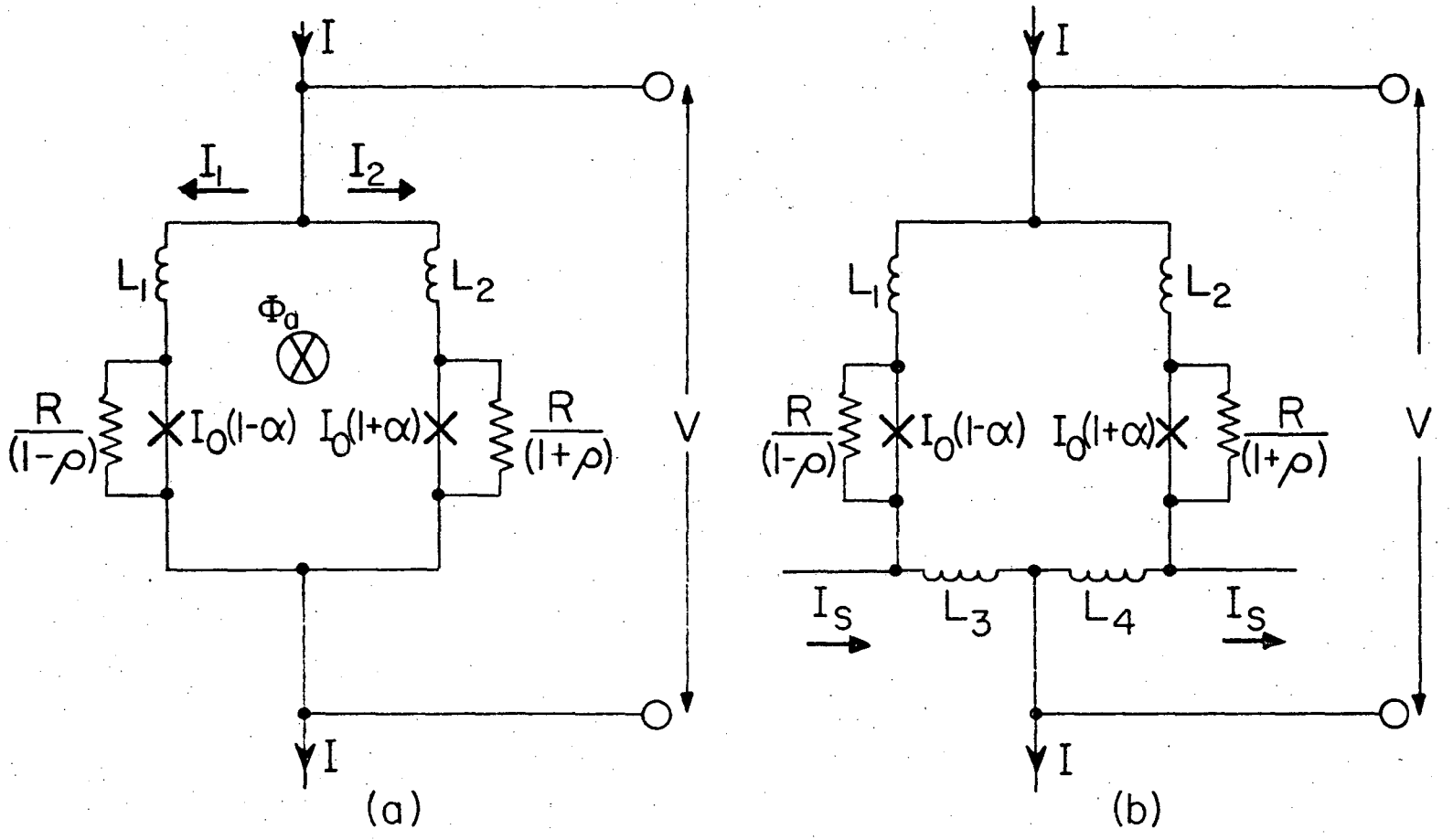

Fig. 1

XBL7611-7729

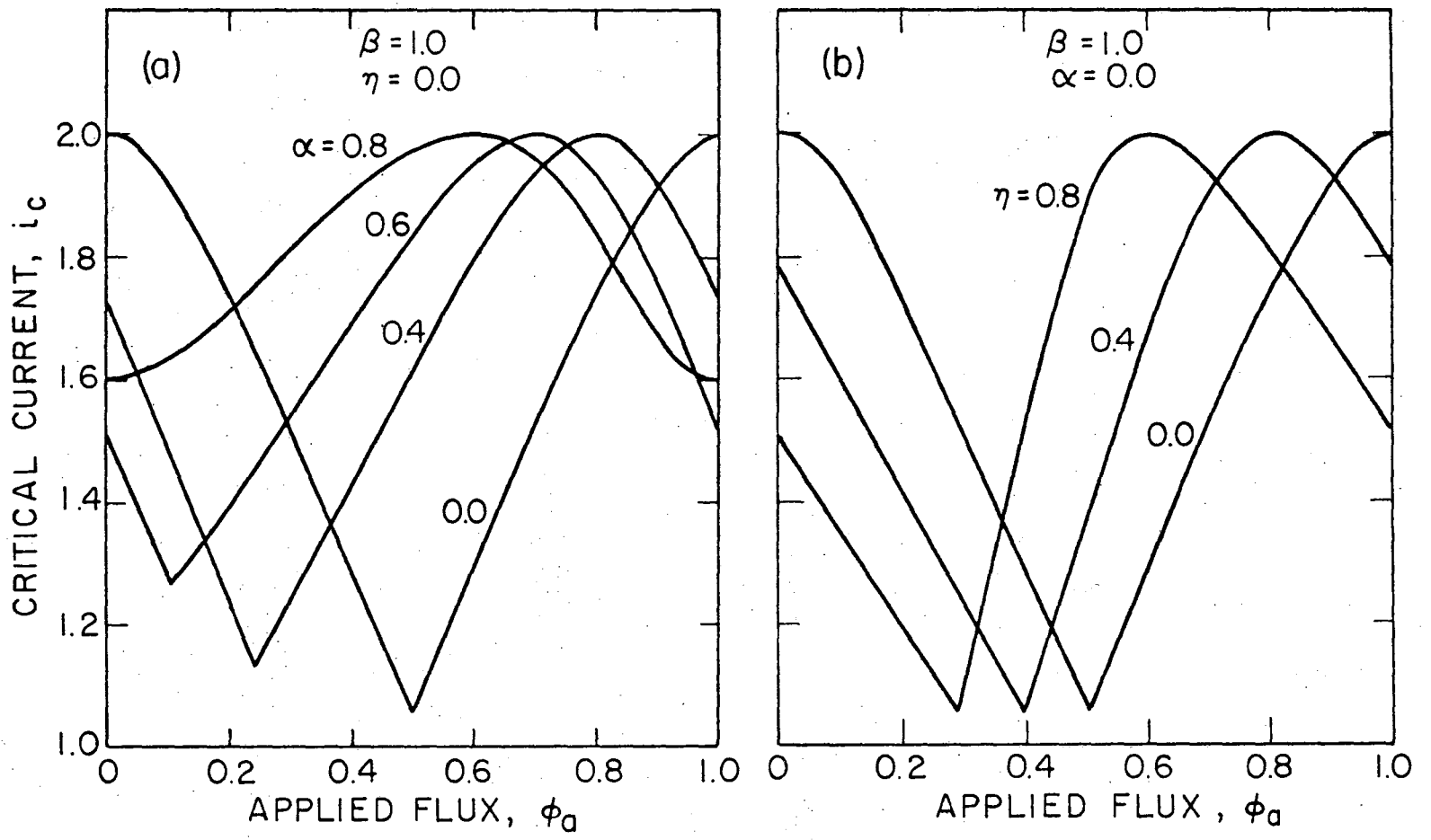

Fig. 2

XBL767-7189

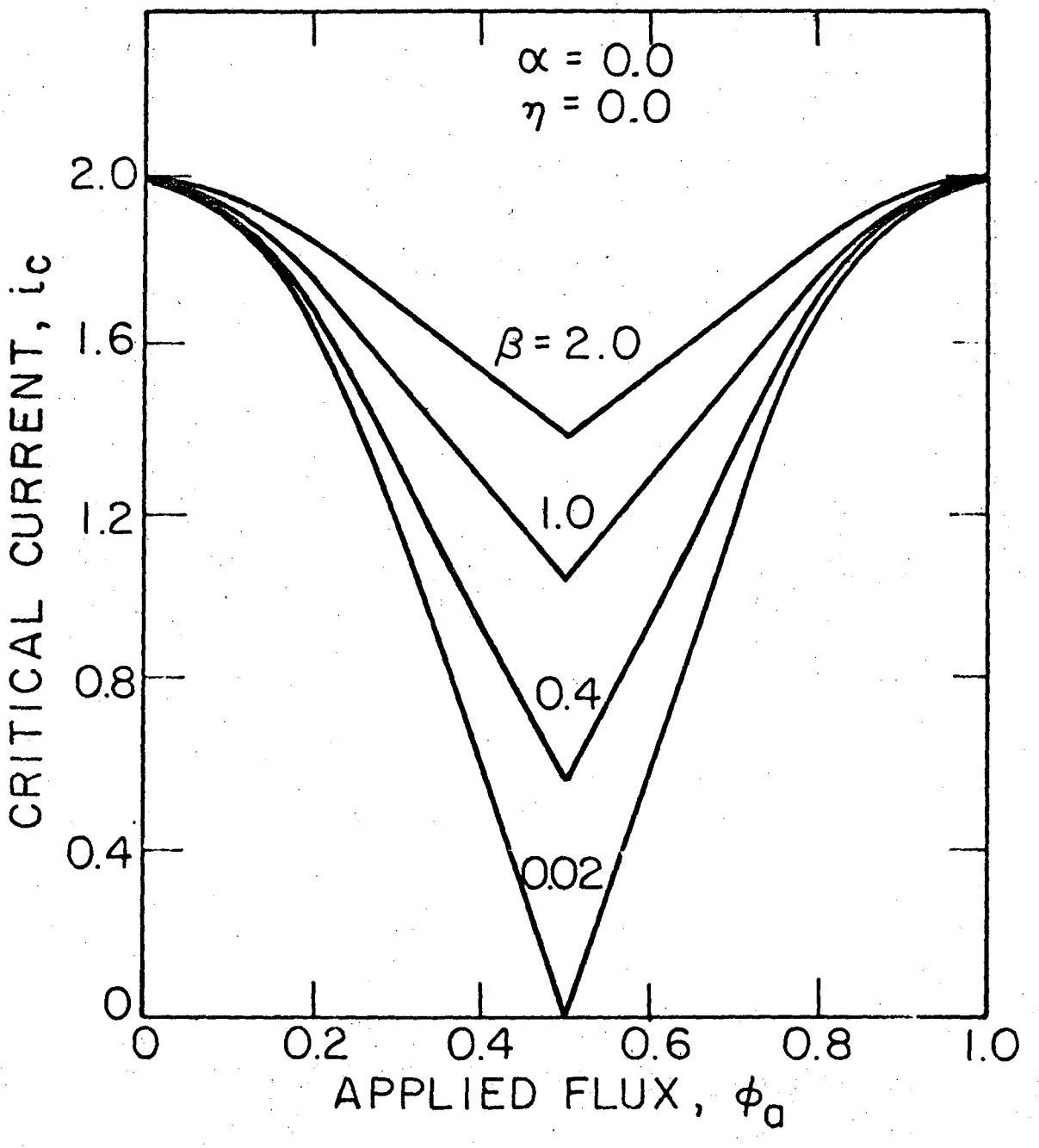

Fig. 3 XBL7612-11,031

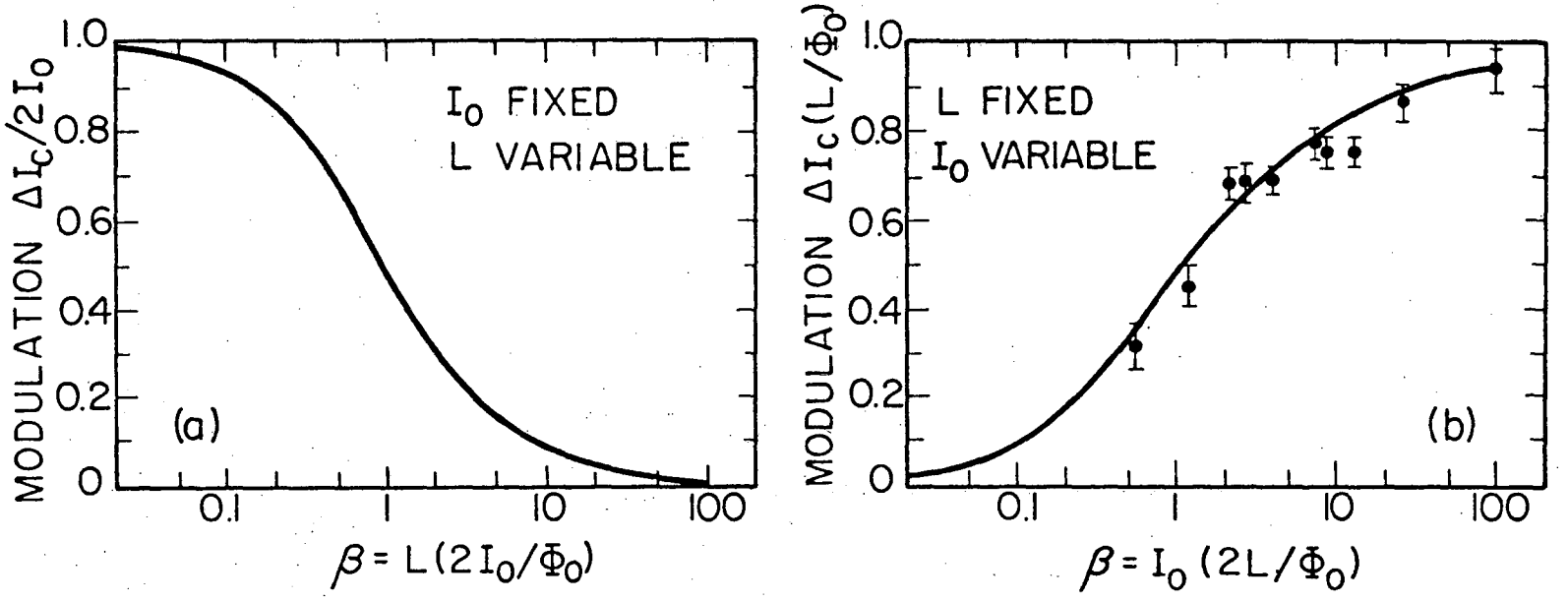

Fig. 4

XBL 7611-7730

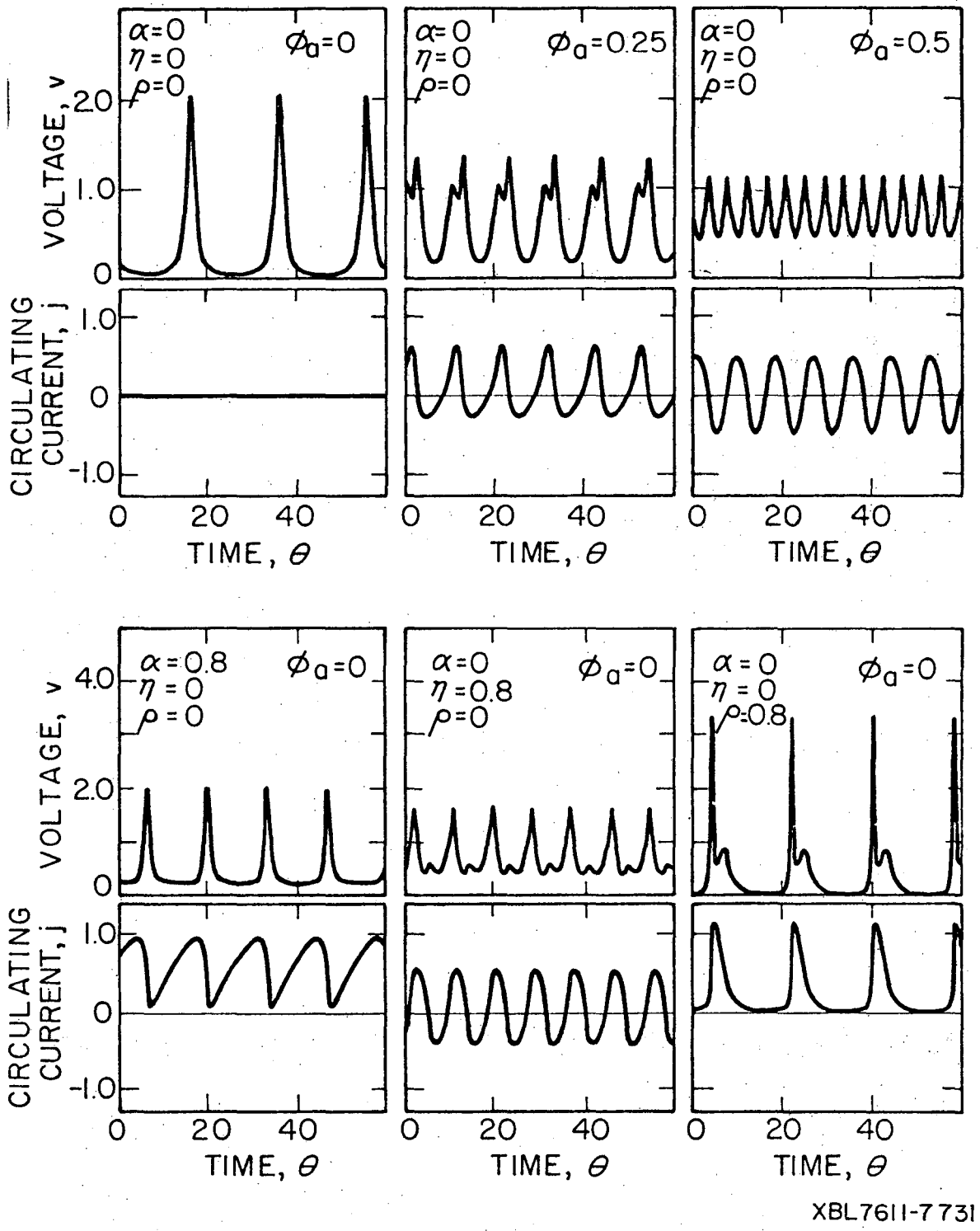

Fig. 5

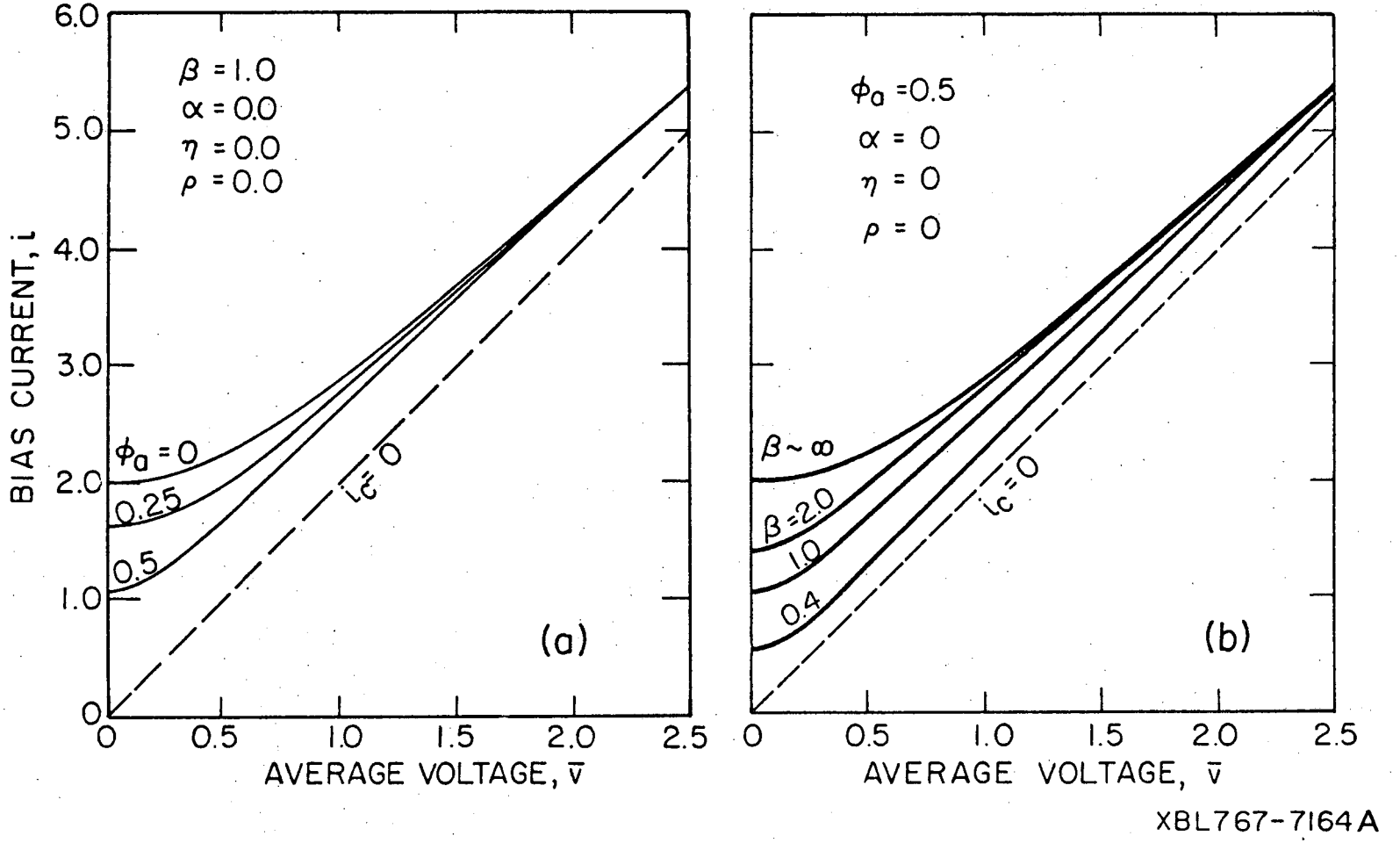
6.0
5.0
4.0
3.0
2.0
1.0
0
BIAS CURRENT, i
β = 1.0
α = 0.0
η = 0.0
ρ = 0.0
φa = 0
0.25
0.5
ic = 0
(a)
0
0.5
1.0
1.5
2.0
2.5
AVERAGE VOLTAGE, v̄
φa =0.5
α = 0
η = 0
ρ = 0
β ~ ∞
β =2.0
1.0
0.4
ic = 0
(b)
0
0.5
1.0
1.5
2.0
2.5
AVERAGE VOLTAGE, v̄
XBL767-7164A

Fig. 6

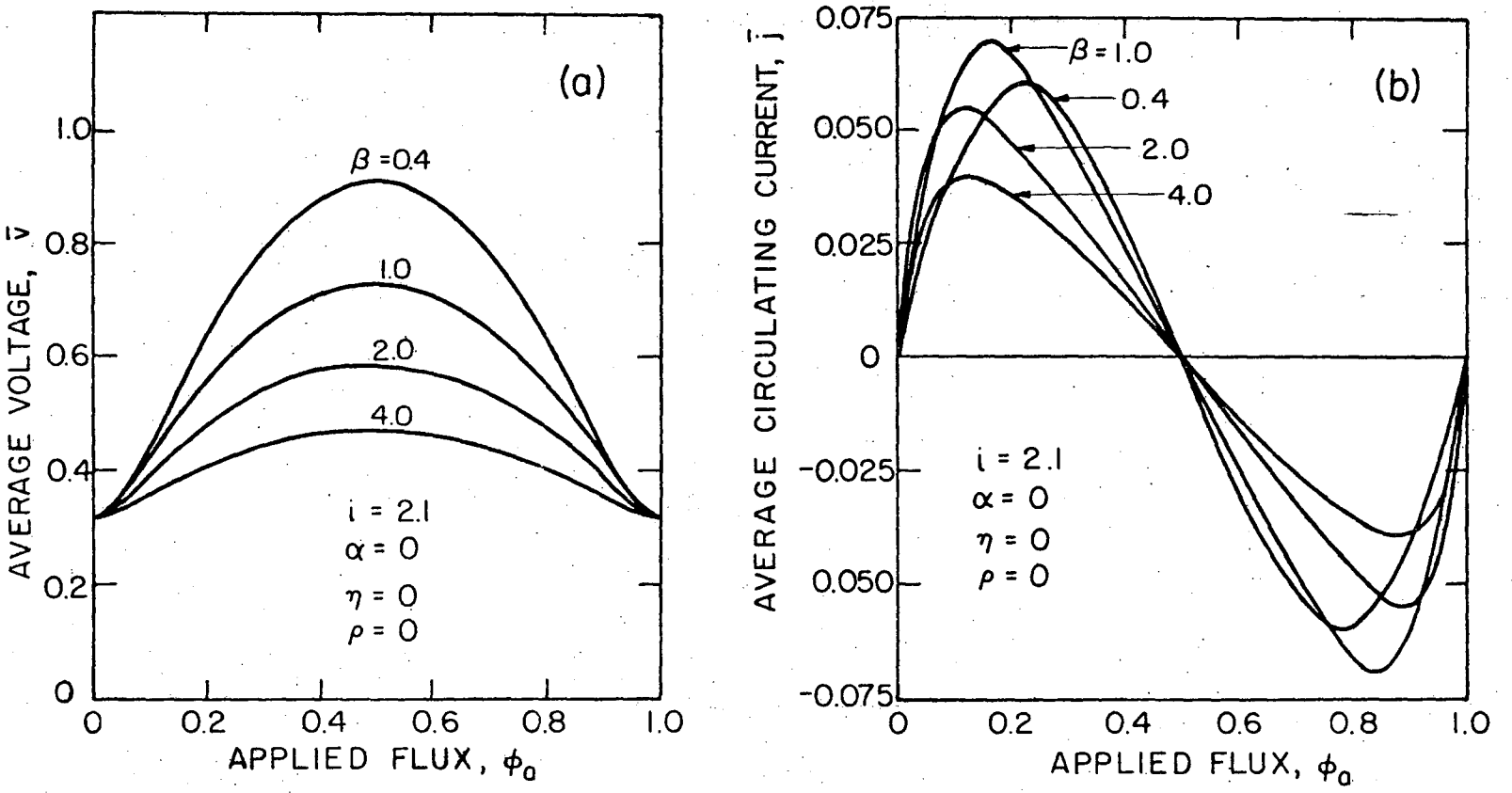

Fig. 7

XBL 767-7167A

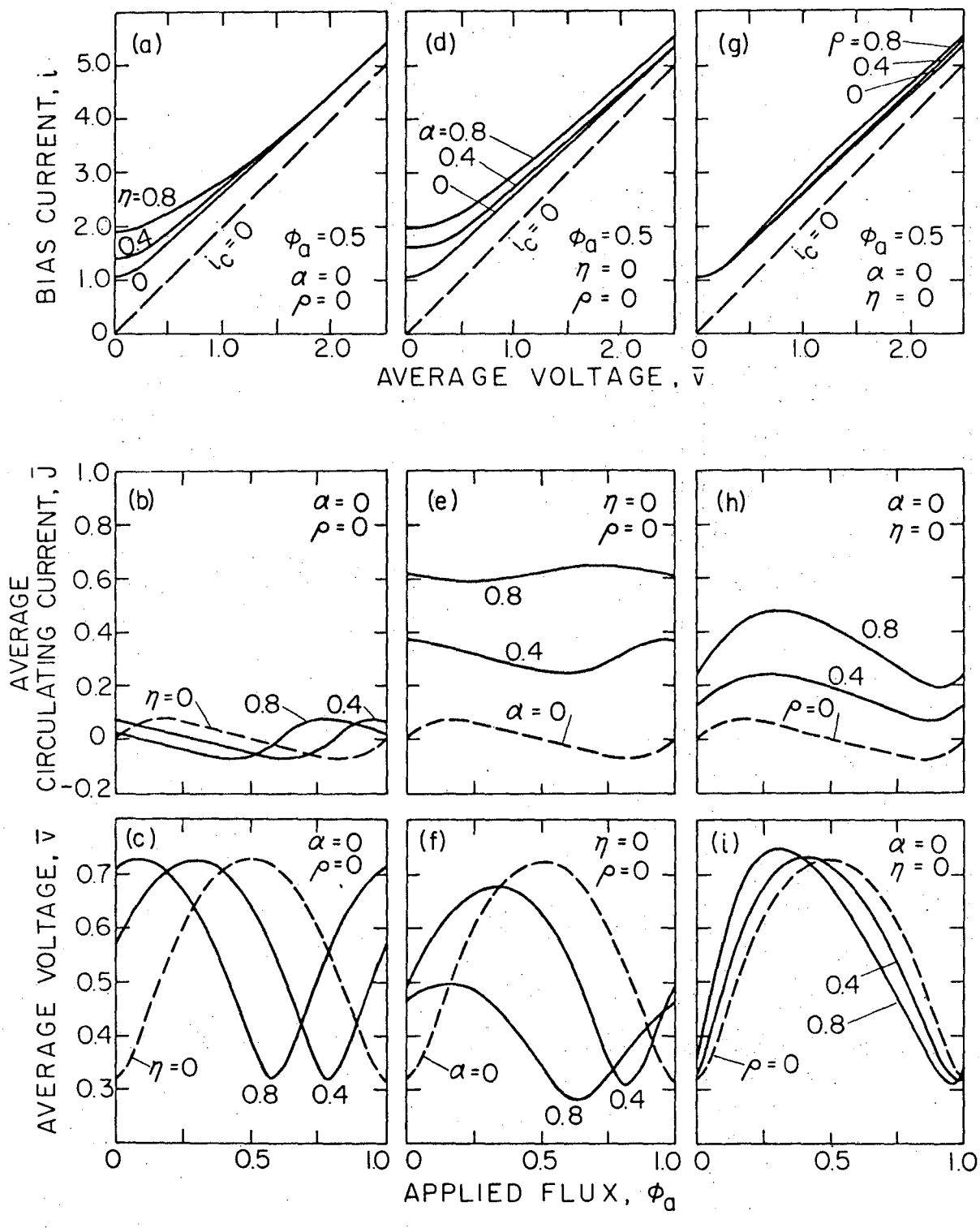
(a)
(b)
(c)
(d)
(e)
(f)
(g)
(h)
(i)
BIAS CURRENT, i
AVERAGE CIRCULATING CURRENT, J
AVERAGE VOLTAGE, v
AVERAGE VOLTAGE, v
APPLIED FLUX, Φa
η=0.8
0.4
0
ic=0
Φa=0.5
α = 0
ρ = 0
α=0.8
η = 0
ρ=0.8
XBL 7612-11,036

Fig. 8

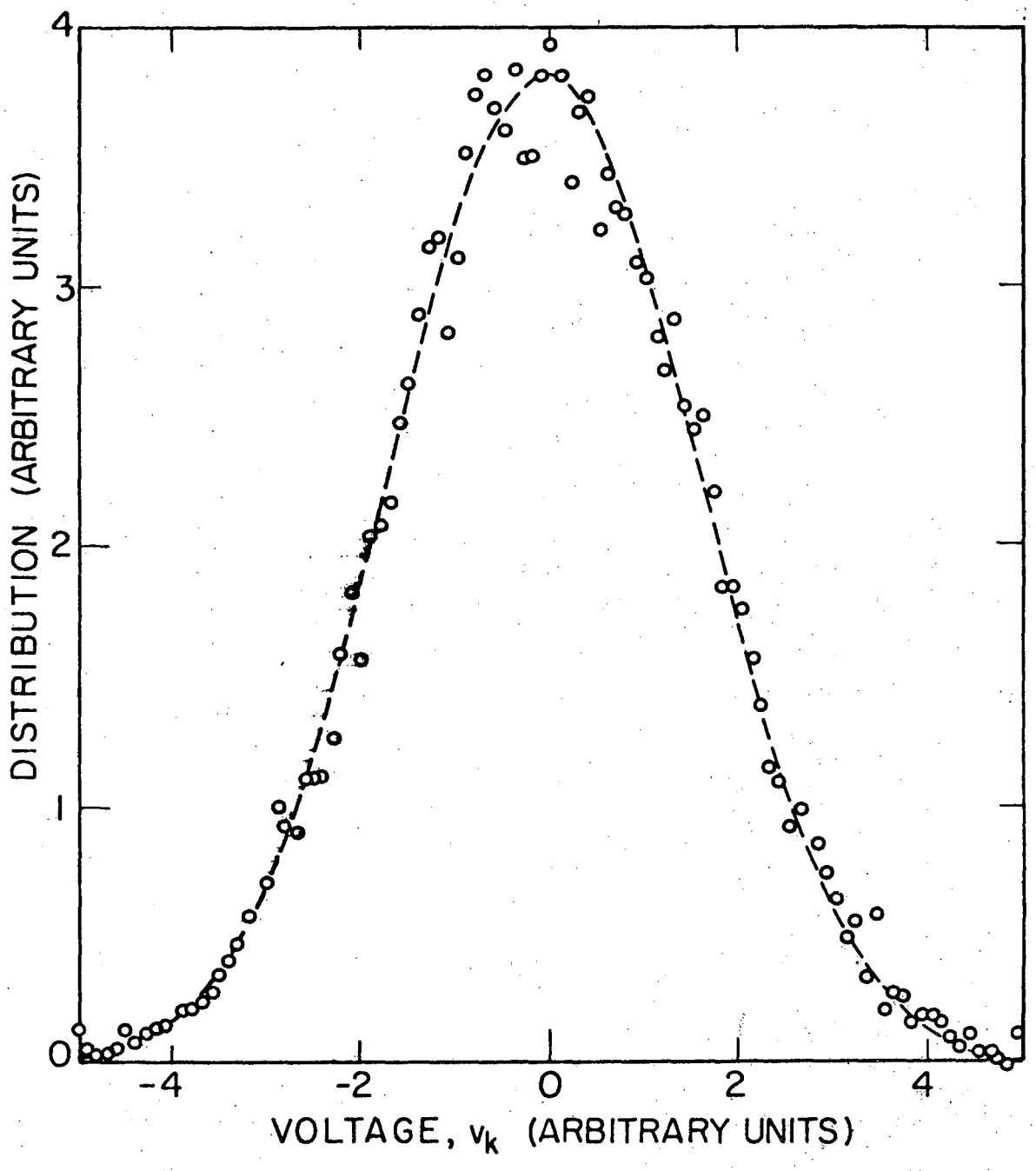

Fig. 9

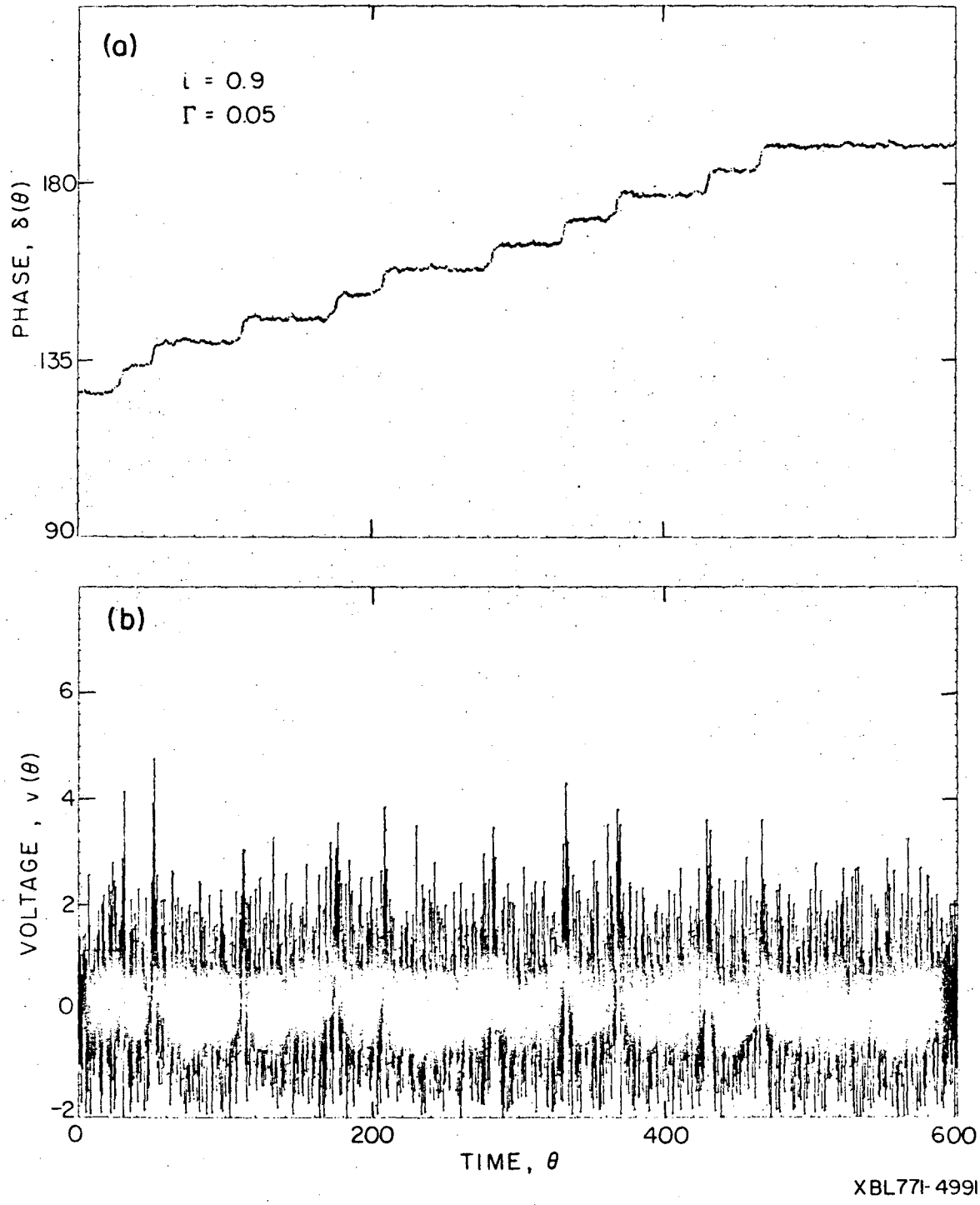
(a)
ι = 0.9
Γ = 0.05
PHASE, δ(θ)
180
135
90
(b)
VOLTAGE, v(θ)
6
4
2
0
-2
0
200
400
600
TIME, θ
XBL771-4991

Fig. 10

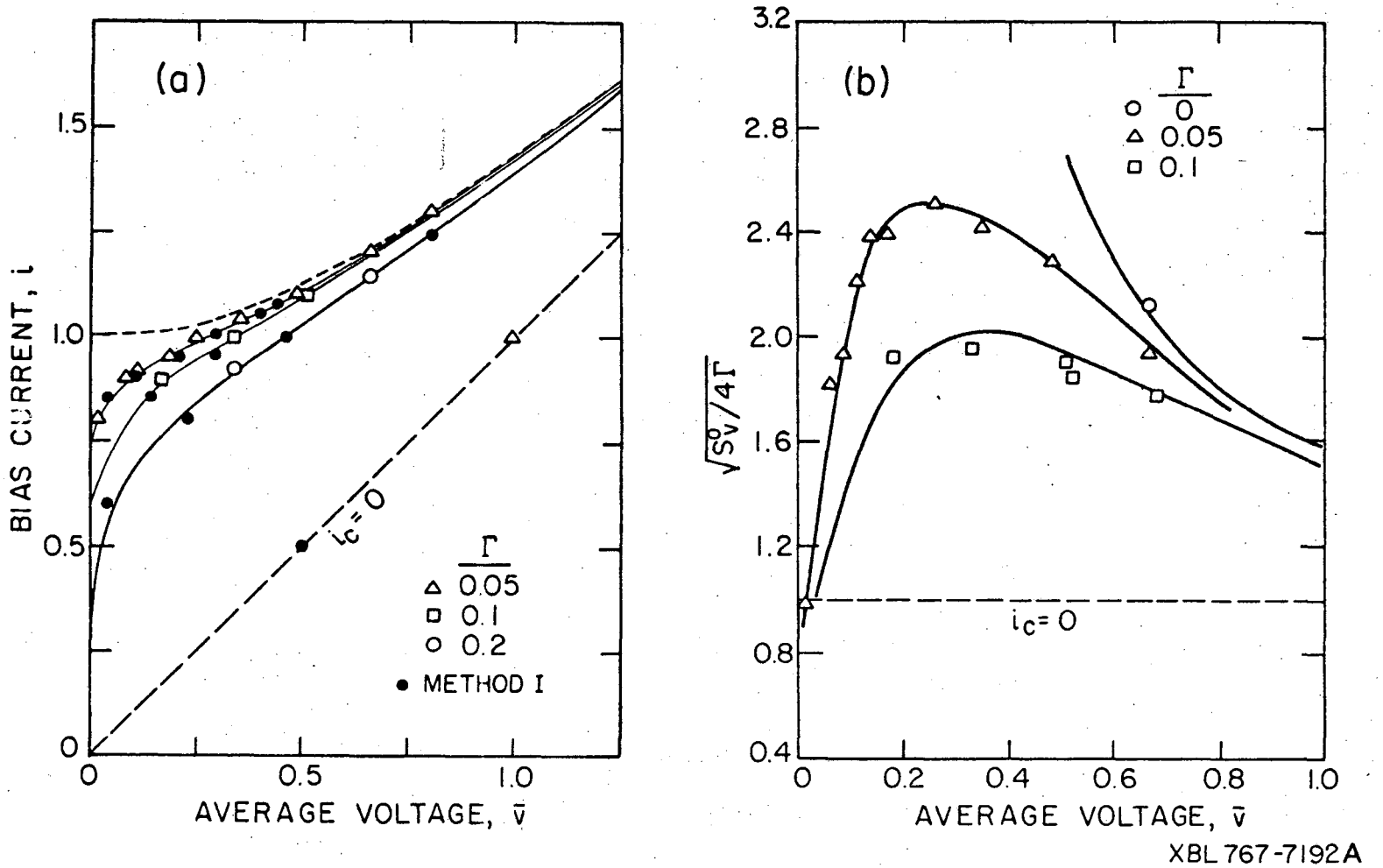

Fig. 11

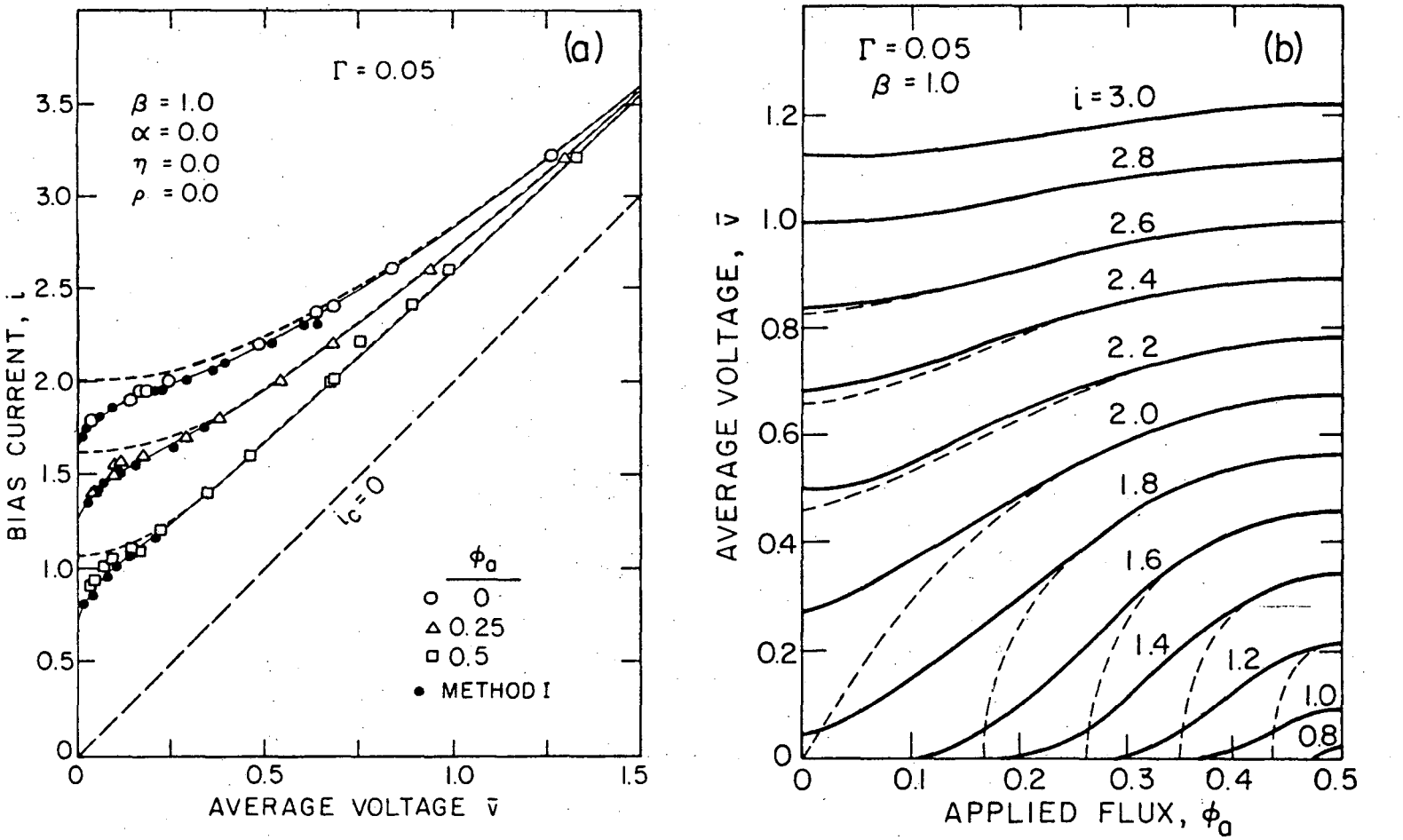

XBL 768-7265A

Fig. 12

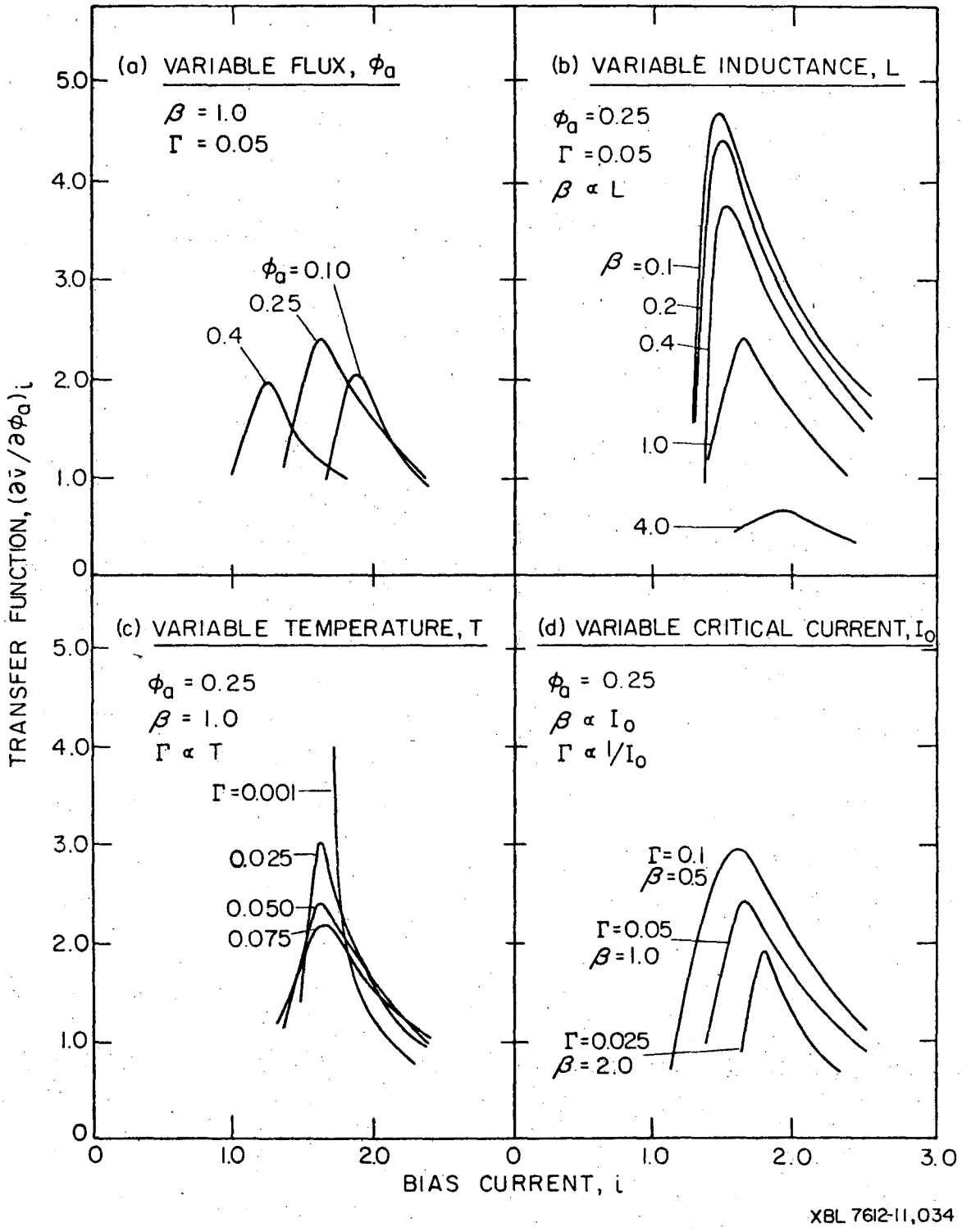
(a) VARIABLE FLUX, ϕ_a
β = 1.0
Γ = 0.05
ϕ_a = 0.10
0.25
0.4
(b) VARIABLE INDUCTANCE, L
ϕ_a = 0.25
Γ = 0.05
$\beta \propto L$
β = 0.1
0.2
0.4
1.0
4.0
(c) VARIABLE TEMPERATURE, T
ϕ_a = 0.25
β = 1.0
$\Gamma \propto T$
Γ = 0.001
0.025
0.050
0.075
(d) VARIABLE CRITICAL CURRENT, I_o
ϕ_a = 0.25
$\beta \propto I_o$
$\Gamma \propto 1/I_o$
Γ = 0.1
β = 0.5
Γ = 0.05
β = 1.0
Γ = 0.025
β = 2.0
TRANSFER FUNCTION, $(\partial \bar{v}/\partial \phi_a)_i$
BIAS CURRENT, i
0
1.0
2.0
3.0
4.0
5.0
XBL 7612-11,034

Fig. 13

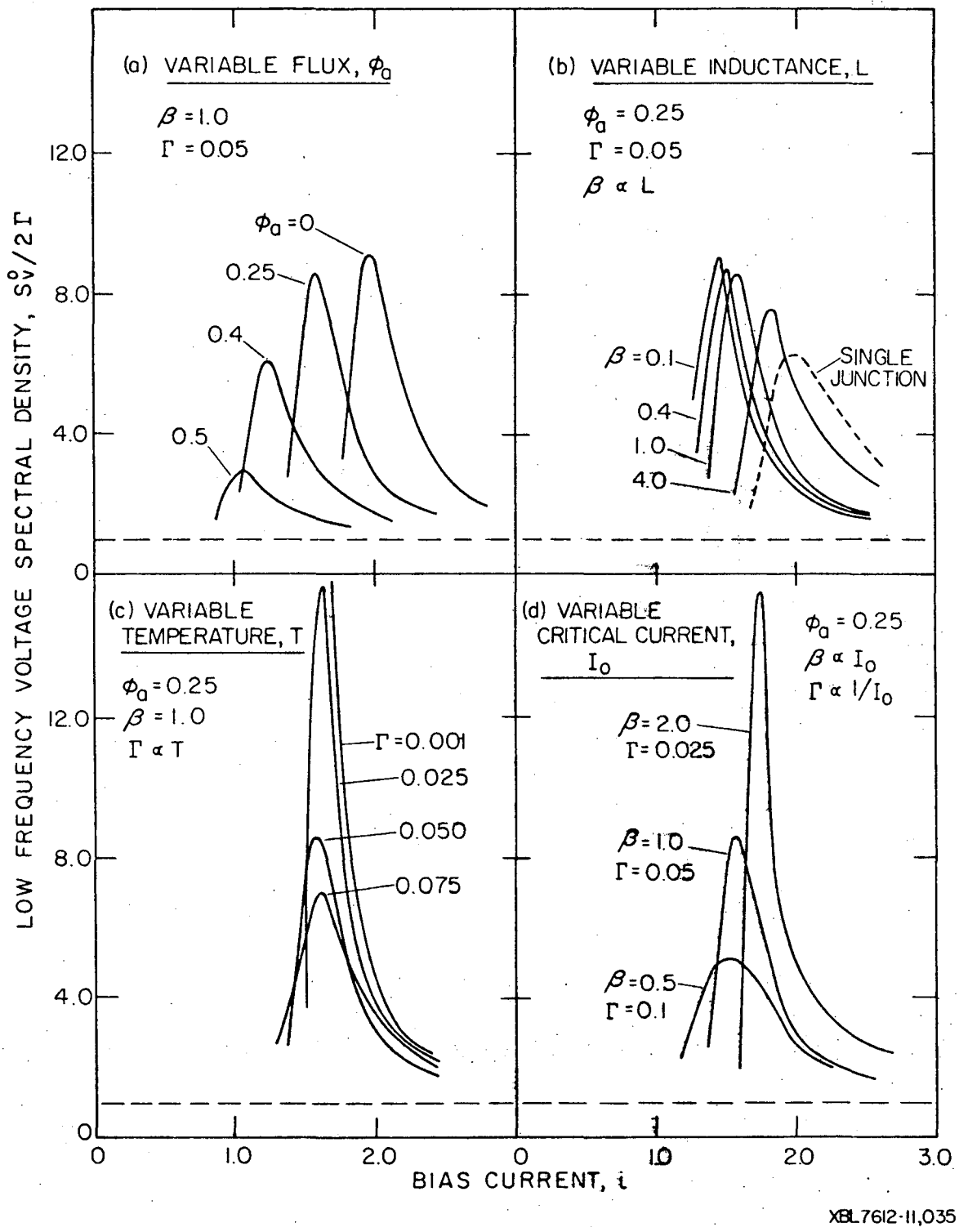

XBL7612-11,035

Fig. 14

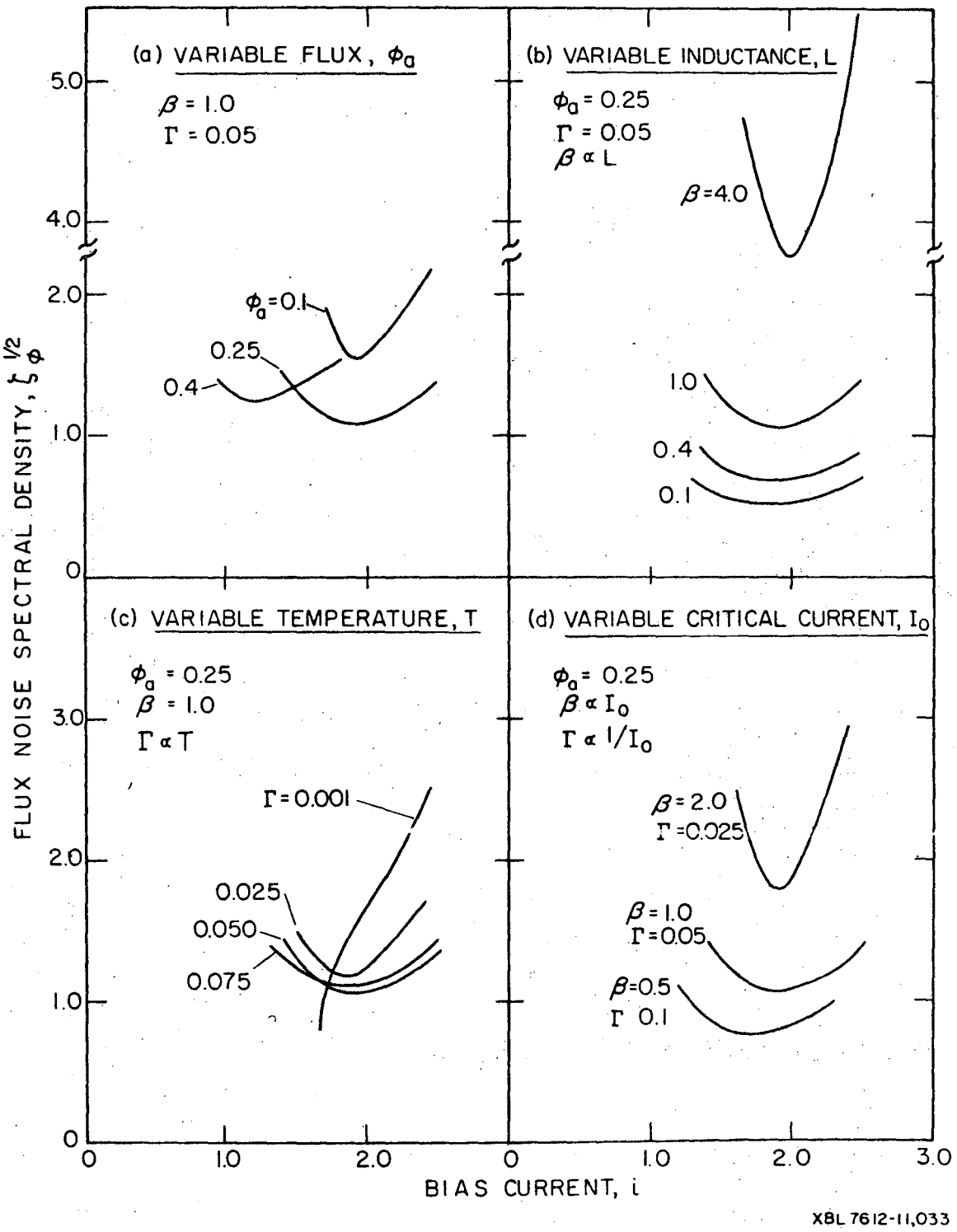
(a) VARIABLE FLUX, ϕ_a
β = 1.0
Γ = 0.05
ϕ_a=0.1
0.25
0.4
(b) VARIABLE INDUCTANCE, L
ϕ_a = 0.25
Γ = 0.05
$\beta \propto L$
β=4.0
1.0
0.4
0.1
(c) VARIABLE TEMPERATURE, T
ϕ_a = 0.25
β = 1.0
$\Gamma \propto T$
Γ=0.001
0.025
0.050
0.075
(d) VARIABLE CRITICAL CURRENT, I_0
ϕ_a = 0.25
$\beta \propto I_0$
$\Gamma \propto 1/I_0$
β = 2.0
Γ =0.025
β = 1.0
Γ =0.05
β=0.5
Γ 0.1
FLUX NOISE SPECTRAL DENSITY, $\zeta_\phi^{1/2}$
BIAS CURRENT, i
0
1.0
2.0
3.0
4.0
5.0
XBL 7612-11,033

Fig. 15

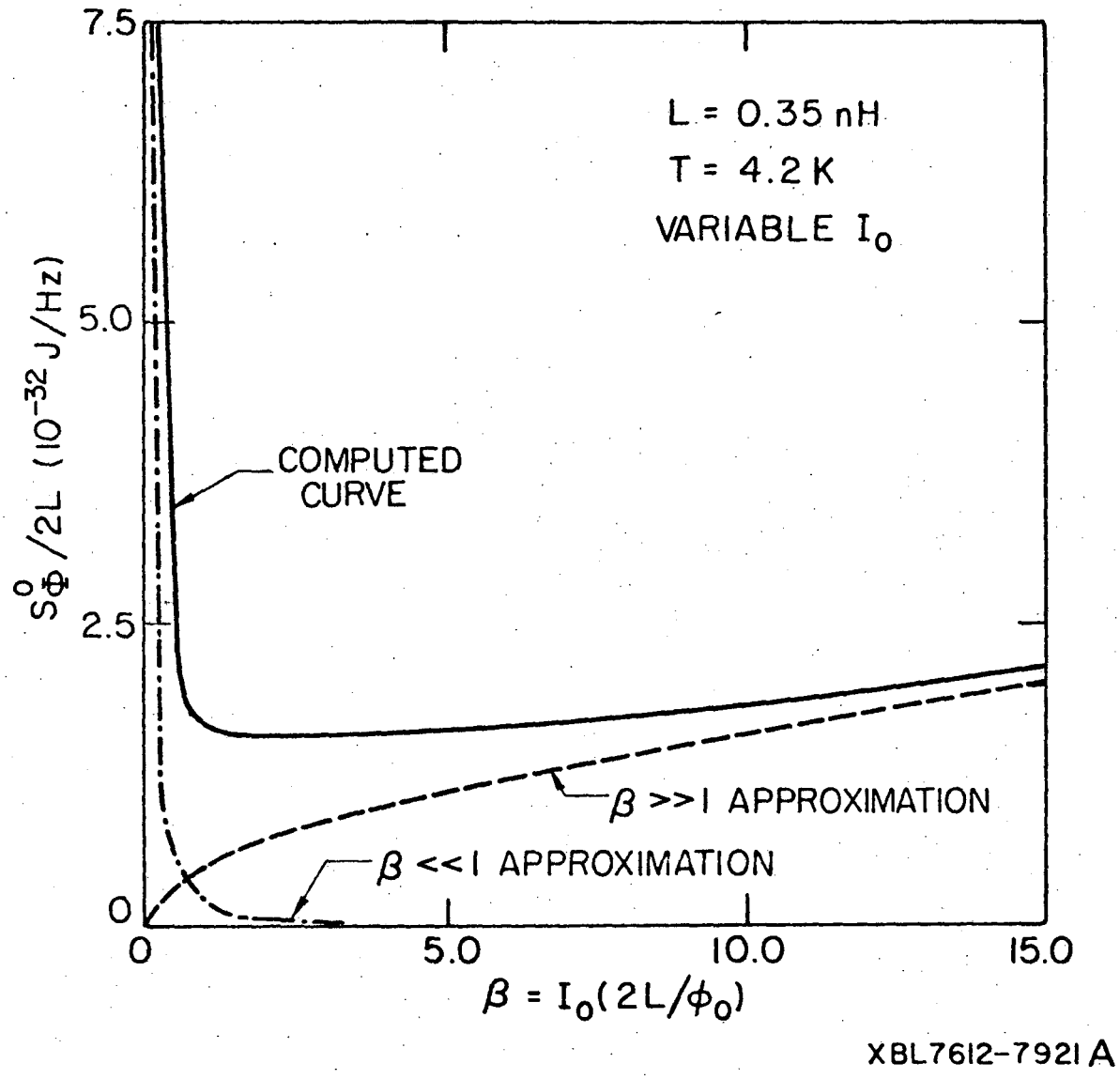
7.5
5.0
2.5
0
0
5.0
10.0
15.0
L = 0.35 nH
T = 4.2 K
VARIABLE I_0
COMPUTED CURVE
$\beta \gg 1$ APPROXIMATION
$\beta \ll 1$ APPROXIMATION
$S^0_\Phi/2L$ (10^{-32} J/Hz)
$\beta = I_0(2L/\phi_0)$
XBL7612-7921A

Fig. 16

This report was done with support from the United States Energy Research and Development Administration. Any conclusions or opinions expressed in this report represent solely those of the author(s) and not necessarily those of The Regents of the University of California, the Lawrence Berkeley Laboratory or the United States Energy Research and Development Administration.

TECHNICAL INFORMATION DIVISION
LAWRENCE BERKELEY LABORATORY
UNIVERSITY OF CALIFORNIA
BERKELEY, CALIFORNIA 94720